FP7-313161

A holistic, scenario-independent, situation-awareness and guidance system for sustaining the Active Evacuation Route for large crowds

OPTIMIZED ROLL-TO-ROLL PRINTING AND RFID TAGS

Deliverable Identifier:	D.7.7
Delivery Date:	Feb, 2016
Classification:	Restricted
Editor(s):	Diego Betancourt (TUD), Marvin Barahona (TUD) and Katherina Haase (TUC)
Document version:	1.2 - 2016
Contract Start Date:	April 1st, 2013
Duration:	48 months
Project coordinator:	EXODUS S.A. (Greece)
Partners:	EXO (GR), IT INNOVATION (UK), ICCS (GR), HKV (NL), TEL (GR), TEK (ES), AIA (GR), VITRO (IT), CDI (UK), INDRA (ES), KUL (BE), DXT (FR), POLITO (IT), STX-FR (FR), TUD (DE), TUC (DE), ASRS (ES), METB (ES), TIM (IT)

Project co-funded by the
European Commission under the
7th Framework Programme

Document Control Page

Title	OPTIMIZED ROLL-TO-ROLL PRINTING AND RFID TAGS	
Editors	Diego Betancourt	TUD
	Marvin Barahona	TUD
	Katherina Haase	TUC
Contributors	Name	Partner
	Diego Betancourt	TUD
	Marvin Barahona	TUD
	Katherina Haase	TUC
Peer Reviewers	Name	Partner
	Jorge Juan Rodriguez Vasquez	INDRA
	Jose Miguel Landeta	TEK
	Daniel Höft	TUC
Format	Text - Ms Word	
Language	en-UK	
Work-Package	WP7	
Deliverable number	D.7.7	
Due Date of Delivery	29/02/2016	
Actual Date of Delivery	4/03/2016	
Dissemination Level	Restricted to other programme participants (including the Commission Services)	
Rights	eVACUATE Consortium	
Audience	☐ public ☒ restricted ☐ internal	
Date	3/03/2016	
Revision	none	
Version	1.2	
Edited by	Diego Betancourt	
Status	☐ draft ☐ Consortium reviewed ☐ WP leader accepted ☒ Project coordinator accepted	

Revision History

Version	Date	Description and comments	Edited by
0.1	07/10/2015	Initial draft	TUD
0.2	08/10/2015	Minor corrections applied	TUD, TUC
0.3	09/10/2015	Table 2.5 updated and links to videos added	TUD, TUC
0.4	27/10/2015	Peer-review comments and corrections added	TUD, TUC
1.0	10/11/2015	Final version	TUD, TUC
1.1	3/03/2016	Updated version, section 3.4 added	TUD, TUC
1.2	8/03/2016	Conclusion section updated, figure 3.1 added	TUD

Table of Contents

Table of Figures

List of Tables

Executive summary

This document deals with the development of the named **“chipless RFID system”**. This report is aligned with the results obtained during the realization of Task 7.6 and is a complement of similar deliverables previously submitted, to known: Deliverable 7.1, Optimization of roll-to-roll printing technology for RFIDs; and Deliverable 7.3, First design of roll-to-roll RFIDs. The main contributors of this deliverable were TUD for the parts related to tag design and reader test-bed development, and TUC for issues related to the tag manufacturing. The report, mainly include the activities performed on Task 7.6 during the project period of time ranging M22 to M35 but some references are made to previously reported work (D7.1 and D7.3). The report is organized as follow: in a first section, the overall chipless RFID system achievements are summarized, then the specific achievements regarding the tag development are introduced and, on the last part of the deliverable, the reader test-bed achievements are reported. Additional documentation and supports of the work done are indexed on the annexes whereas the specific files are uploaded to the eVACUATE SharePoint.

1 Chipless RFID system

1.1 Description

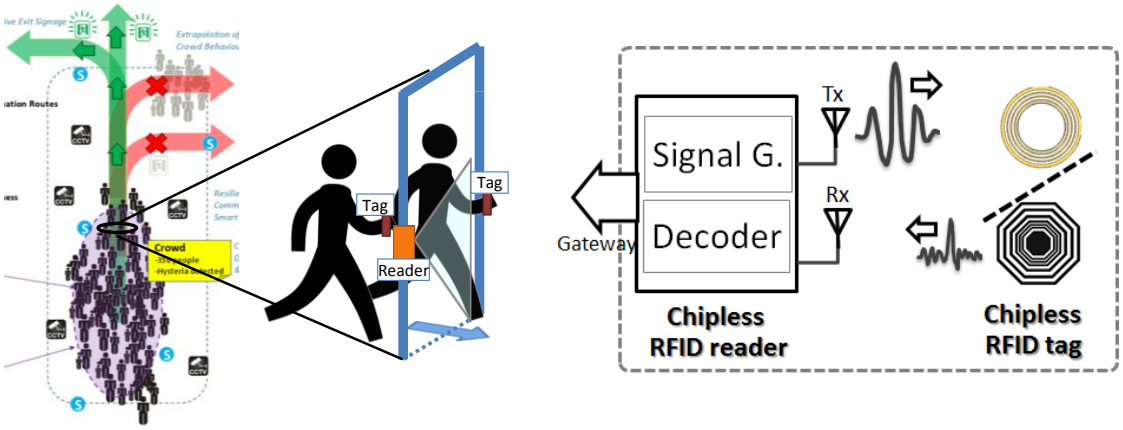

a b

Figure 1-1. a)The chipless RFID system as a part of the Active Evacuation Route. b) The chipless RFID system architecture.

The chipless RFID system provides to the eVACUATE's framework the number and type of persons that have crossed through a particular position (gate) at the venue. Up to 8 different groups of persons are planned to be identified by using this system, namely: Elderly persons, babies, children, pregnant women, disabled persons, first actuators, staff and others. The information provided by the system could be used to update and maintain the Active Evacuation Route (AER) defined for a specific venue (see Figure 1-1a). This system is based on a very novel approach that combines the use of radar technology with radio frequency identification methodologies at a very low cost per tag. The chipless RFID system is composed by the chipless RFID reader and the chipless RFID tag. A block diagram for the whole system architecture is shown in Figure 1-1b.

The chipless RFID reader is, in fact, an adapted version of an Ultra-Wide-Band (UWB) frequency radar [Karm13]. The main function of the reader is to send a pulse to excite the tag and to collect the backscattering signal from it. Additionally, the reader contemplates a digital processing unit responsible for the processing of the received signal and the extraction of the information stored on the tag, as well as the communication unit to connect the system to the eVACUATE's framework.

The chipless RFID tag is an inexpensive, passive and fully printed device responsible to store the information that identifies the type of person crossing through a gate. The information is stored in the tag by using the resonant features of the geometry of the tag [Nair14, Nair14a]. The tags were produced with a range of printing inks and mass-production compatible methods to ensure the low cost per tag.

1.2 Specifications and overall achievements

The design requirements as described in the eVACUATE project's DoW are summarized in the Table 1-1. All the actions devoted to fulfill the requirements defined in the project DoW for the chipless RFID system are included into the Task 7.6. This framework task was divided in specific sub-tasks, each one following the goals as described in the same table.

Table 1-1. eVACUATE chipless RFID system targets according to the DoW

Parameter		Min	Typ	Max	Units
Cost of chipless RFID tag				0.01	€/30cm^2
Life-time of chipless RFID tag		3			months
Reading range[1]			1		m
Tag DC power consumption			0		V
Number of bits		3			bits
Pilot test	Anoeta Stadium		YES		
	Athens Airport				
	STX's cruise ship				
	Bilbao's Metro Station				

1. Is the maximum distance to which the chipless RFID tag reader can successfully detect the chipless RFID tag

The minimum possible price of the chipless RFID tags is assured by the use of both, a mass production fabrication technique and cheaper substrate materials. In particular, R2R printing technologies were used to manufacture the tag while inexpensive flexible materials as paper and plastic were used as substrates for the same. More detailed information on this regard is shown in section 2.3. However, the targeted price of less than 1 Euro cent per tag cannot be achieved with the current designs. It is noticeable that much of the tag's price is only due to the amount of silver-ink used and thus, different functional materials to be used in the tag's printing process need to be considered. For this purpose, alternative materials including copper-based inks and foils were explored. The achievements on this regards are introduced in section 2.4.

The usage of environmentally stable printing ink ensures the proper functionality of the chipless RFID tags over the desired life time of 3 months (see section 2.2.1). In addition, the eventuality of adding a coverage layer to the tags is considered in section 2.2.1.1. The main results obtained in this regard, corroborates that it is possible to laminate the printed tags without disturbing the original performance of tags while the durability of the tags is increased.

Since the chipless RFID tags are conceived as a pure passive device which do not include any surface mount device (SMD) or integrated circuit (IC) on it, there is no power consumption and thus the 0 Volts of power consumption are assured.

The read range target (1 m) is a key point in the design of the chipless RFID for eVACUATE project. During the tag design stage, the reading range is directly related to the Radar Cross Section (RCS) feature exhibited by any chipless RFID tag. In this way, the enhancement of the RCS implies an increment on the associated read range. For this purpose, innovative design methodologies are applied on the tags designed for eVACUATE. The results obtained in laboratory (at anechoic chamber) demonstrated that a read range up to 1.8 m is achievable [Beta14], in addition to this, by using the experimental results, a maximum read range of about 3.5 m is estimated (see section 2.1.1).

The number of bits requested by the application is quite low; just 3 bits are needed to codify the 8 different groups of individuals to be identified by the chipless RFID system. Currently, the latest tag designs selected to be used during the test pilots of eVACUATE project, named

the octagonal and circular chipless RFID tags, can codify 5 and 3 bits, respectively (see sections 2.1.1 and 2.1.2 for more details). Notwithstanding this requirement is fulfilled, it is in the interest of the consortium to explore possibilities to develop a high capacity tag in order to promote a probable future commercialization of the eVACUATE project outcomes. To give a response to this necessity, a novel tag design based on advanced optimization techniques was proposed. This tag is based on the Genetic Algorithm (GA) design and can provide a design with an expected capacity ranging from 8 to 14 bit. The initial results and a proof of concept are introduced in the section 2.4.3.

Additional performance tests, regarding the effects of basic deformations introduced to the tags (bending and folding) as well as the effects of human body on the tags are discussed in sections 2.2.2 and 2.2.3, respectively.

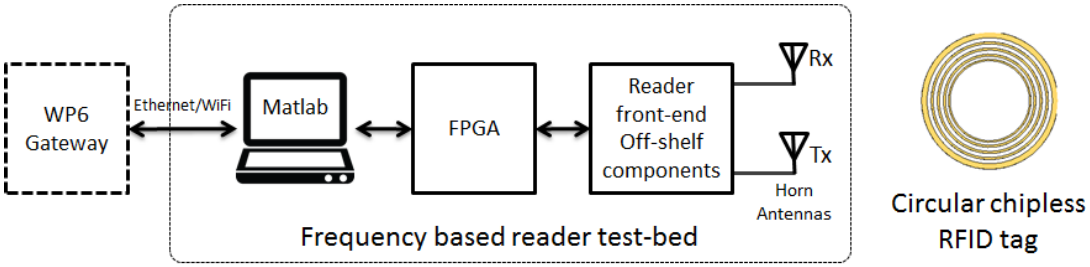

Figure 1-2. frequency based reader test-bed schematic diagram

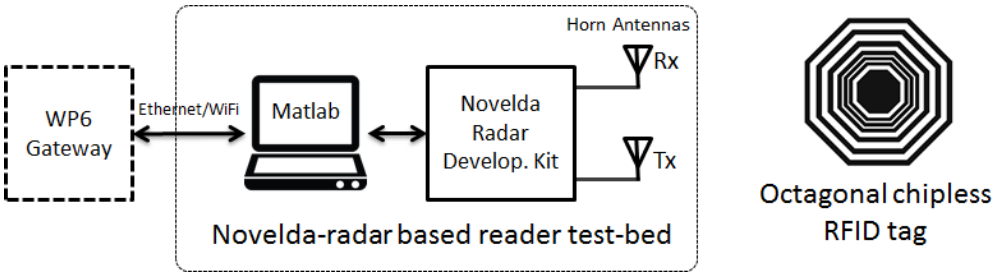

Figure 1-3. Novelda-radar based reader test-bed

Finally, in order to test the chipless RFID system during the pilot tests planned for the eVACUATE project, a proof-of-concept system was developed. The proof-of-concept includes all the necessary elements to create a functional and stand-alone chipless RFID system to be placed and tested at the venues wherever the pilot-test takes place. The proof-of-concept device is composed by a reader test-bed and a set of chipless RFID tags. The chipless RFID tags used within the proof-of concept include both the octagonal tag and the circular tag. Both tags are codified for 8 different IDs as required in this specific application. The reader test-beds developed for testing purposes include two different versions: the frequency based reader and the Novelda-radar based test-beds.

The frequency domain reader is based on a frequency modulated continues-wave (FMCW) interrogation signal which sweeps the frequency band between 4 and 6 GHz in order to obtain the correspondent tag's characteristic. This reader is meant to be used with the correspondent designed circular tags as depicted in Fig. 1-2.

On the other hand, the Novelda radar works in the time domain generating a short pulse (in the order of picoseconds) which is then backscattered by the tag, since the working frequency of the Novelda radar is from 4 to 8 GHz, the octagonal tags are used in conjunction with this one as shown in Fig. 1-3.

The development of the reader test-bed's decoding techniques as well as the presentation of the graphical user interface of the reader's consoles and reading results are introduced in section 3.

2 Chipless RFID tags

2.1 Tag design and fabrication

This section contemplates the realization of both: the octagonal chipless RFID tags and the circular RFID tags (version 2). In the same way, detailed information about the tag's fabrication process is provided.

2.1.1 Octagonal chipless RFID tag

For further information about the design process and codifying methodology employed, please refer to the D7.3.

Table 2-1. Octagonal chipless RFID tag specifications

Electrical Specifications					
Parameter		Min	Typ	Max	Units
Coding Capacity[1]			5		bits
Frequency of operation		4		10	GHz
Polarization dependence			NO[2]		
RCS		-35		-15	dBsm
Read range (estimated –peak)[3]				3.5	m
Read range (estimated –Notches)[4]		1			m
Min bent curvature radius allowed[12]		16			cm
Min fold angle allowed[13]		45			deg
Reader-TB Compatibility	Novelda		YES		
	Frequency		NO		
Mechanical Specifications					
Parameter		Min	Typ	Max	Units
Size of tag		23 x 23[11]	52 x 52	52 x 82	mm^2
Compatibility with mass production			YES[5]		
Substrate Thickness	PET[6]		100		µm
	Paper[7]		100		µm
Estimated price[8]		0.0334			€/27cm^2
Morphological characterization of printed area					
Substrate		PET	Paper		Units
Conductor thickness (d)		4.29 ± 0.51	4.39 ± 0.77		µm
Roughness (Ra)[9]		0.87 ± 0.19	1.11 ± 0.30		µm
Roughness (Rz,din)[9]		3.63 ± 0.59	4.12 ± 0.67		µm
Sheet resistance ($R_{\blacksquare}$)[10]		0.11 ± 0.021	0.11 ± 0.005		Ω/sq
Electrical conductivity (σ)		20,602 ± 3,952	20,910 ± 1,358		S/cm
Printing Accuracy Δx		8.63	1.60		%
Printing Accuracy Δy		5.41	1.72		%

1. See Figure 2-5
2. Measured at 0 deg, 45 deg and 90 deg.
3. For a 3dBm power source. See Figure 2-2
4. For a -10dBm power source. See Figure 2-2
5. Screen printing methodology was used
6. Melinex® 401 CW PET 100 µm (DuPont Teijin Films)
7. Maxipgloss 135 g/m² (Igepa)
8. Depending on the conductor thickness (d). based on ink price of 950 €/Kg (see section2.3)
9. determined by profilometry at DEKTAC 8M (VEECO)
10. Van-der-Pauw method
11. See Figure 2-1
12. See Figure 2-3
13. See Figure 2-4

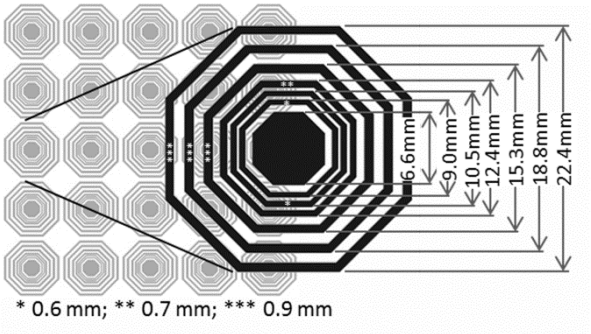

Figure 2-1. Octagonal chipless RFID tag (in the background) and the unit element (in the foreground) and its dimensions

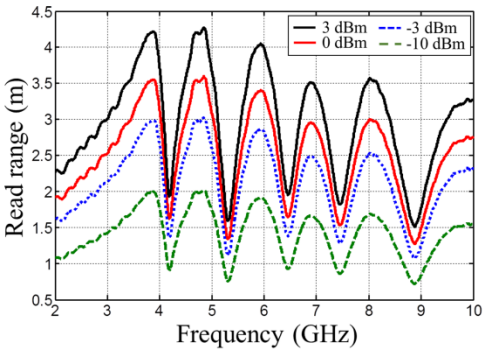

Figure 2-2. Read range estimated by using experimental data and the radar equation [Tay12].

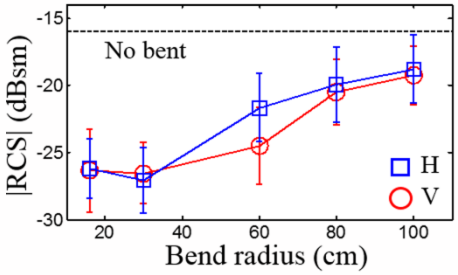

Figure 2-3. Averaged RCS vs bend radii measured for a bent tag. In the graph, the reference level of the tag unfolded/non-bent is included as a dashed line.

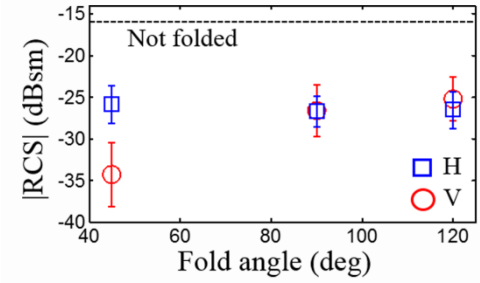

Figure 2-4. Averaged RCS vs folded angle measured for a folded tag. In the graph, the reference level of the tag unfolded/non-bent is included as a dashed line.

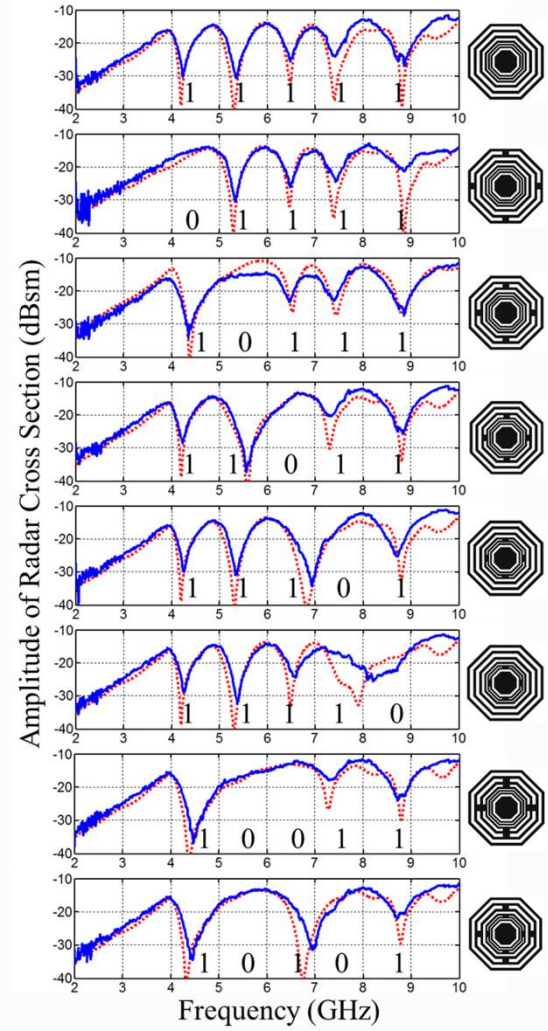

Figure 2-5. |RCS| measurement for the eight (out of 32 possible) different IDs octagonal chipless RFID tags. Solid line for measurements, dashed line for simulations. The correspondent ID is indicated in each sub plot as well as the unit element base for the tag.

2.1.2 Circular chipless RFID tag version 2

The circular chipless RFID tag version 2 is depicted in Figure 2-6a, it follows the same design principle as the one presented in Deliverable 7.3 but with a shift in frequency of 900 MHz to the higher frequencies in order to achieve a working bandwidth from 4 to 6 GHz. Additionally, a coding of up to 3 bits is designed by means of the peak-frequency shift coding shown in Figure 2-6b. That is, a peak shifted to the left represents a zero, and a peak shifted to the right represents a one for the given bit.

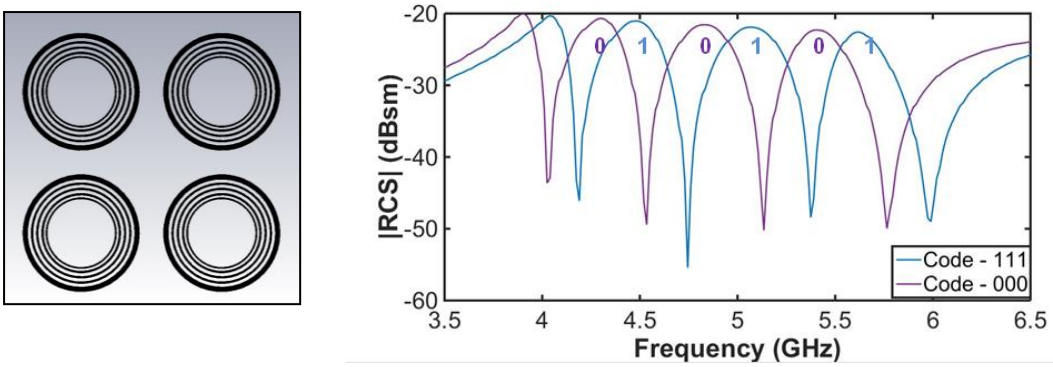

(a) (b)

Figure 2-6. (a) Circular Tag Design 2 (b) Coding principle

The shift in the peaks is achieved varying the different resonators radii, separations and widths. The dimensions of each tag code are shown in Table 2-2. A minimum width of 0.3 mm is designed as well as a minimum separation of 0.2 mm.

Table 2-2. Circular Tags Design 2 physical dimensions R1 = radius of resonator 1, Smn = separation between resonators m and n, and Wn = with of resonator n

Dimension	Code1	Code2	Code3	Code4	Code5	Code6	Code7	Code8
R_1 (mm)	11.8	11.6	11.8	11.9	12	12.2	12.2	12.2
S_{12} (mm)	0.7	0.6	0.7	0.7	0.7	0.7	0.7	0.7
S_{23} (mm)	0.6	0.8	0.7	1.3	1.3	0.7	0.7	1.4
S_{34} (mm)	0.5	0.3	0.7	0.7	0.3	0.7	1.0	0.7
S_{45} (mm)	0.8	0.4	0.4	0.4	0.2	0.5	0.5	0.3
W_1 (mm)	1.0	1.1	1.0	0.5	1.0	1.0	1.0	0.6
W_2 (mm)	0.4	0.3	0.4	0.4	0.4	0.4	0.4	0.5
W_3 (mm)	0.3	0.3	0.4	0.4	0.5	0.4	0.3	0.4
W_4 (mm)	0.4	0.4	0.4	0.4	0.3	0.4	0.5	0.3
W_5 (mm)	0.3	0.3	0.3	0.3	0.3	0.3	0.3	0.3

The measurement results are shown in Figure 2-7. As can be seen, most of the tag follow the design pattern but for a frequency shift of around 200 MHz to the lower values. Additionally, codes 2, 5 and 8 present some deviations from the simulated response. Considering code 2, the dip formed between the first two peaks and for code 5 the second peak are not well developed. Therefore, both tags appear similar in signature as shown in Figure 2-8a, and thus they could be counted as only one code depending on the detection algorithm. In the case of code 8, there has been a fabrication variation with respect to the original design

which changed the last peak position, generating a frequency response almost identical to the one from code 4 as can be seen in Figure 2-8b. Therefore, it can be concluded that the concept of this design has been proofed. However, additional adjustments in order to eliminate the aforementioned deviations will be required.

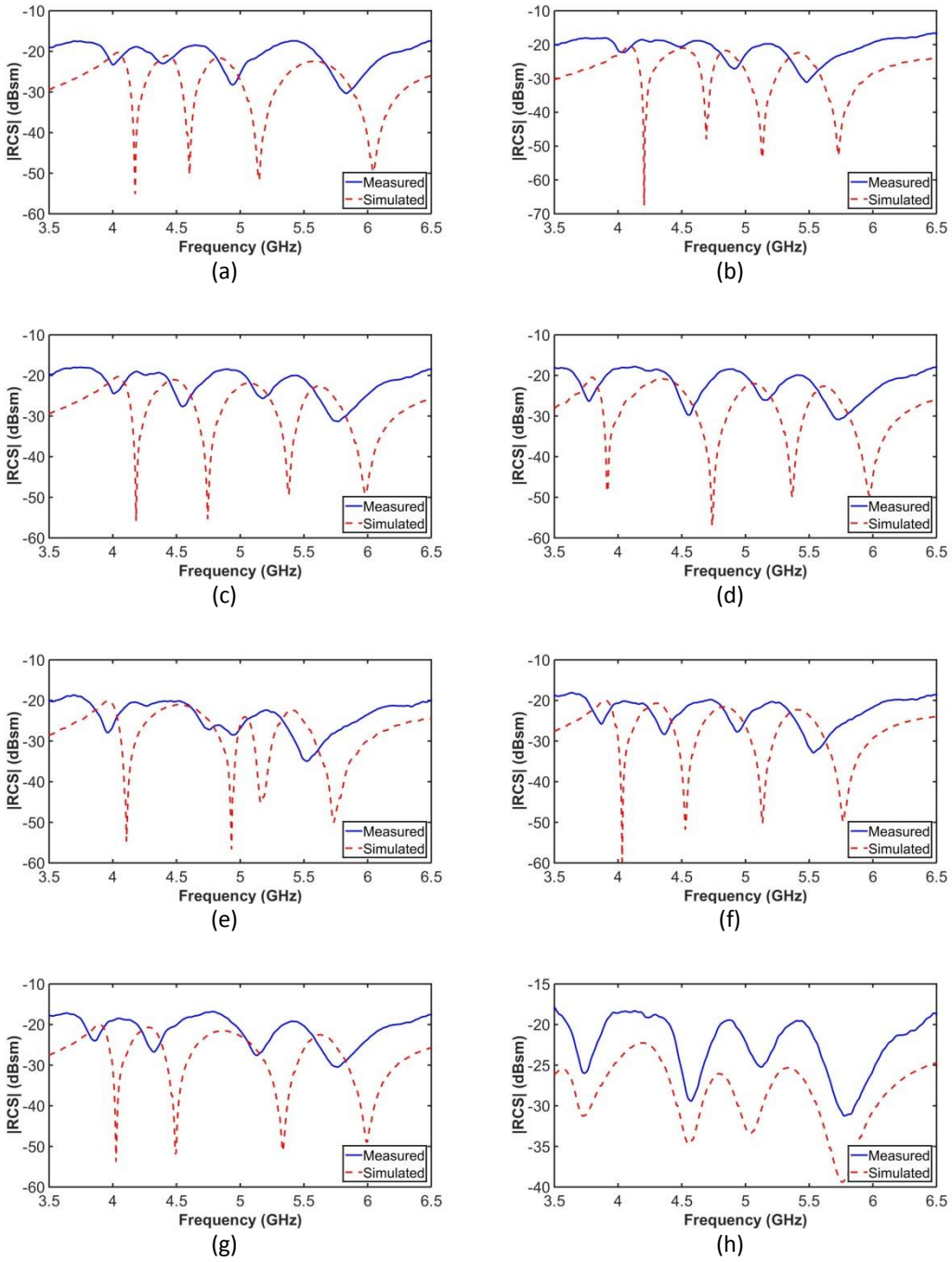

Figure 2-7. Comparison of circular tag's measurements of a four periods tag against simulations made for one period of (a) code 1, (b) code 2, (c) code 3, (d) code 4, (e) code 5, (f) code 6, (g) code 7, and (h) code 8.

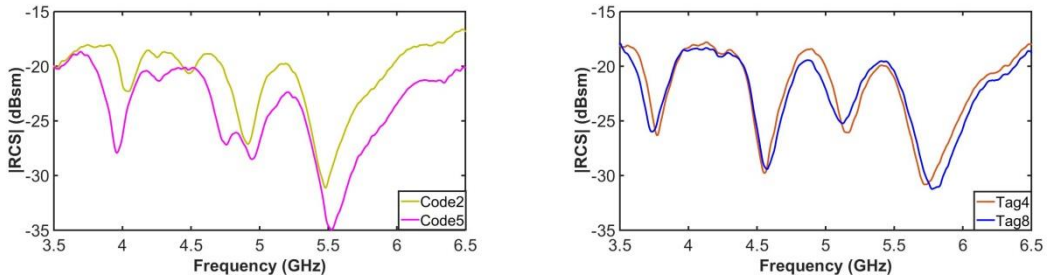

(a) (b)

Figure 2-8. Similarities between codes (a) 2 and 5, (b) 4 and 8.

2.1.3 Printing of octagonal and circular (version 2) chipless RFID tags

In order to estimate the potential of each printing technique, the conductivity of the material was determined and used as the basis to identify the required conductor thickness, which will be needed for the particular application (frequency bandwidth: 3.1…10.6 GHz). In general, a printing technique that is suitable to produce relatively thick lines needed to be selected in order to minimize losses and ensure good performance of the chipless RFID tag [Man09],[Fei07].

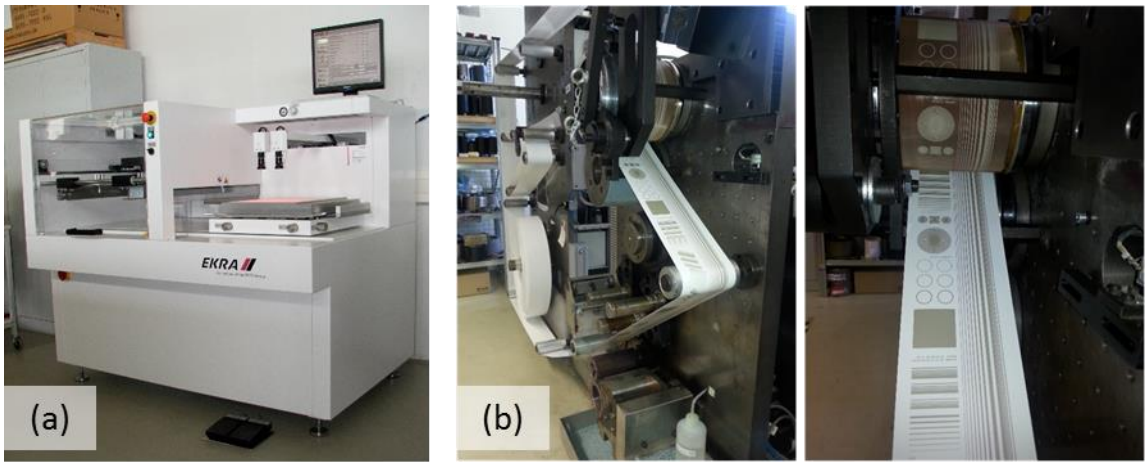

Figure 2-9. Utilized screen printing machines: (a) sheet-fed screen printer EKRA X1 SL, (b) Rotary Screen Printing Unit at Laboratory Printing Machine Laborman I

Therefore, octagonal and circular (version 2) chipless RFID tags were produced by screen printing as it was found to fit best with the thickness requirements of the conductive film. As high conductivity was found to be indispensable for achieving the designed functionality, silver-particle based printing paste was utilized to produce octagonal and circular chipless RFID tag designs. In order to find a good compromise between film thickness, structure width and the accurate reproduction of fine lines, a printing screen with a mesh count of 120 L/cm and a thread diameter of 34 µm was selected (SEFAR PET®1500: 120-34 [Bot_]). Sheet printing tests and test samples were produced at the semi-automatic sheet-fed screen printer EKRA X1 SL as shown in Figure 2-9(a). Roll-to-roll printing capability was tested and assessed by respective rotary screen printing tests at a laboratory printing machine (Laborman I). Roll-to-roll printing was performed with a customized printing cylinder fitting

the requirements of the rotary printing machine. Furthermore, for the production of roll-printed films, the use of an adapted ink, modified with 10% thinning solution, was found to provide positive effects on the printing result. Both, sheet printing tests and rotary screen printing were performed at a speed of 100 mm/s. While printed sheets were sintered offline (box oven) at 120°C for 6 minutes, the roll-printed layers were dried inline with the hot air drying system set to 140°C (~25 s). Test prints were performed on paper (Igepa Maxigloss 135 g/m²) and foil (100 µm PET - Melinex® 401) substrates.

At this point it should be further mentioned that for the realization of former tag designs, roll-to-roll flexography was proved as possible alternative to the herein applied rotary screen principle. Further details on the printing setup are presented in deliverable D7.1.

2.1.3.1 Tags on various substrates

As it is known from research on printed UHF antennas, the electrical properties of the printing substrate affect the performance of the RFID tag. The loss tangent and relative permittivity of the flexible printing substrates are usually different from conventional substrates, like FR-4, and thus, differences of the performance have to be expected. Particularly considering the most common substrate in printing industry, namely paper, characteristics, such as the porosity, absorptive capacity or thickness, may affect tag performance. Also an indirect impact may be expected as ink transfer and film formation on paper differs compared to non-absorbent, non-porous materials.

Table 2-3. Properties of typical end-user substrates

Type	Description	printing area [cm²]	Thickness [µm]	Grammage [g/m²]	Density [kg/m³]	Porosity (Air permeability)*
Real Sociedad de Futbol (ASRS)						
Entrance Ticket	Thermo-active paper, one side coated	106	110	100	930	< 0.11
Associate Card	Smart card	ID-1	800	-	1390	Non-porous
Athens International Airport (AIA)						
Boarding Pass	Thermo-active paper, one side coated	~165	135…195	120…170	880…910	< 0.16
Baggage Tags	paper	61…120	130…300	135…300	860…1200	< 0.11
Metro Bilbao [METB]						
Ticket[1]	Thermo-active paper	N/A	135	120	905	< 0.11
STX Cruise Ship (STX)						
Associate Card	Smart card	ID-1	950	-	1470	Non-porous

* Bendtsen (DIN 53 120 T1)

Therefore, the expected variations related to the printing substrate were assessed on the basis of the provided end-user materials as used in respective pilot venues. In deliverable 7.1 it was concluded that there is a large variation of expected substrates and additional work should focus on their impact and possible strategies to align them with the concept of eVACUATE system. In this regard, the end-user substrates have been further examined with

[1] Samples of this venue not available, alternative material tested

regard to the characteristics that were suggested as possible impact factors on the printing and functionality of the chipless tags. The respective properties are summarized in Table 2-3.

Table 2-4. Characteristics of selected test samples

Type	Description	Thickness [µm]	Grammage [g/m²]	Density [kg/m³]	Porosity (Air permeability)*	Roughness [µm]	Water absorbency** [g/m²]
A	Standard Office paper	110	90	800	5.37	5.2	15.6
B	Commercial print paper 1 (uncoated)	110	100	900	0.56	5.8	16.4
C	Commercial print paper 2 (gloss finished)	100	135	1300	< 0.11	1.8	18.4
D	Art paper (matt finished)	180	200	1100	< 0.11	2.9	20.6
E	Carton (matt finished)	285	300	1035	< 0.11	2.8	29.2

* Bendtsen (DIN 53 120 T1) **W_A ($Cobb_{10}$) top face (printing surface) (DIN 53 132)

Table 2-5. Height images, thickness and conductivity of conductive films on tested substrates

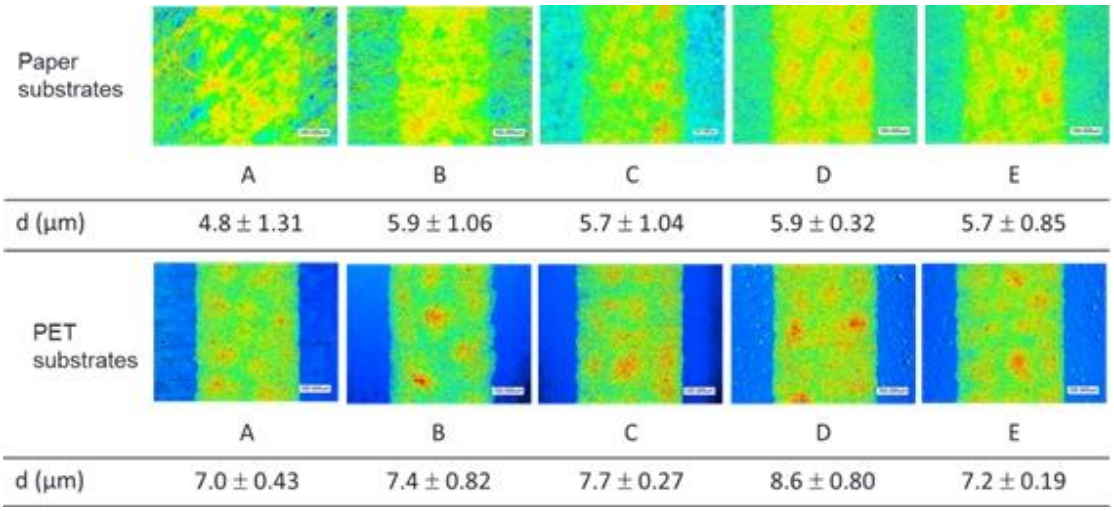

As can be seen, major differences occur with regard to the substrate's thickness and density. Differently, the porosity of all the substrates is found to be rather low and water absorbency is expected to be less as most of the substrates are coated. Considering the associate cards, a major restriction for the integration of chipless tags is given by the available printing area.

As a result of the analysis, it was concluded that the wide range of materials had to be subject of further studies in order to give recommendations for the use in eVACUATE system. Therefore, adequate test samples were selected and assessed with regard to their impact on the production as well as on the chipless tag functionality. The characteristics of the substrates are summarized in Table 2-4.

In addition to the paper samples, test samples with various thicknesses of PET were produced. The respective thicknesses were 50 µm (A), 100 µm (B/ reference), 175 µm (C), 190 µm (D) and 250 µm (E). The density of the PET is around 1.4 g/cm³.

The characteristics of the printed structure on each of the testing material are summarized in Table 2-5. The slight differences, which are recognized with regard to the achieved layer thicknesses are associated to the different surface and wetting properties of the substrate and are considered for tag evaluation in terms of the resulting resistance and related conductivity differences. In particular, slight differences of the RCS magnitude and dynamic margin are expected as a result of the print quality. Other differences should be associated with regard to the differences of the substrate's properties.

In order to evaluate the RCS, octagonal-shape chipless RFID tags were printed on the various substrates and characterized. A comparison of the RCS can be found in Figure 2-10 (a).

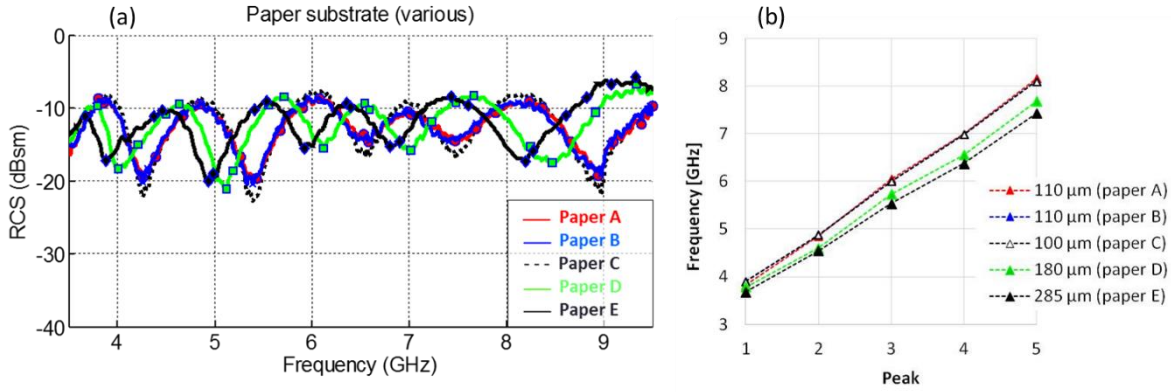

Figure 2-10. (a) RCS for 8 unitary elements and (b) peak frequencies of octagonal chipless RFIDs on a variety of paper substrates

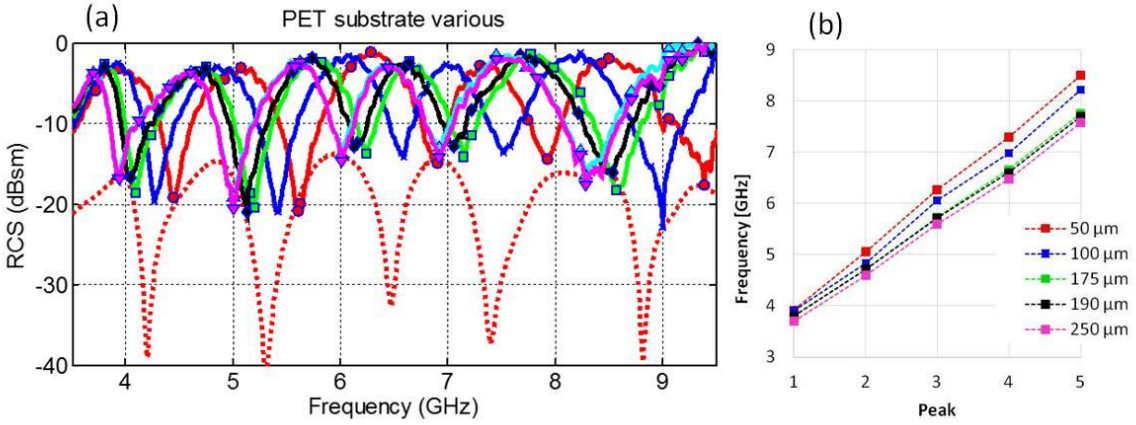

Figure 2-11. (a) RCS for 16 unitary elements (red dashed line: simulation of 4 unitary element tag) and (b) peak frequencies of octagonal chipless RFIDs on PET with various thickness

Considering the differences in terms of porosity, which can be found between paper A, B and C, an impact of this characteristic on the performance of the octagonal tag cannot be

found. Moreover, the density of the paper does not seem to affect the expected behavior, as can be concluded from the comparison of paper A and C. Differently it occurs for the paper thickness. If comparing the results obtained with papers C, D and E, a frequency shift towards lower frequencies can be observed as the thickness increases. This effect is mainly associated to the change of the effective permittivity. In particular, as the thickness is increased, the effective permittivity is expected to increase, which causes a shift of the response to lower frequencies. Nevertheless, an impact of the water absorbency which increases along with the paper's thickness cannot be excluded.

In Figure 2-10 (b), the frequency was plotted for the single peaks of the frequency signature for the various paper substrates. This depiction further exemplifies that the shift in frequency is more distinct at higher frequencies than at the lower frequency range. As depicted in Figure 2-11, similar behavior is observed for the PET samples.

As an outcome of this analysis, it can be concluded that tags, printed on end-user substrates, show the expected behavior and the respective code can be determined from the measured radar cross-section. Nevertheless, smaller variations due to the different characteristics of the substrates and corresponding ink films have to be expected, but can be corrected by the alignment of the tag dimensions. In particular, small reduction in size can be used to shift the peaks/ notches to the initial position. The necessity of this action however depends on the capabilities of the reader.

2.2 Tag performance

2.2.1 Life time of chipless tags

The life time of the printed tag is determined by the exposure to particular external factors that may modify the tags characteristics, in particular conductor and substrate properties, and therefore change the response of the device. With the awareness of possible performance degradation due to environmental and mechanical impact, the materials need to be assessed accordingly. Considering the selected ink, a change in electrical properties smaller than 10% and an insignificant change of physical properties are stated by the ink manufacturer after applying the following commonly utilized environmental testing procedures: [Dup_]

- Thermal Shock: simulation of thermal variations that may be observed during shipping or usage of products
- High temperature aging (dry heat): simulates long term application in high temperature storage conditions
- High temperature/ humidity: simulates long term application in high humidity environments

These environmental testing procedures basically consist of resistance measurements of a well-defined test structure composed of the conductive material to be assessed, which is exposed to particular environmental conditions over a certain period of time. Thereby, the stability or sensitivity of the material to the applied conditions is expressed as percentage change in resistance. Taking into account the respective values as provided by the supplier, **proper functionality of the chipless RFID tags over the desired life time of 3 months, should be ensured** and not impaired by environmental conditions, such as humidity and temperature.

In addition to aforementioned environmental conditions, mechanical stress, applied to the tag, may be a critical influence changing or impairing the chipless tag functionality. The quality of the ink film to sustain mechanical impact is usually tested by the ink manufacturer during standardized adhesion and abrasion tests. The ink manufacturer of the herein utilized ink has been following the procedures according to the American Society for Testing and Materials (ASTM). With an abrasion resistance, expressed in terms of pencil hardness (H) of ≥ 2, and no silver transfer during abrasion/ tape pull test, the utilized material is very well suitable for the use on tickets and similar products.

Nevertheless, additional testing was performed with the aim to predict potential problems due to the target usage of the produced tags. Therefore, an abrasion tester (prüfbau Quartant) has been used to observe the changes of tag and test structures due to mechanical abrasion. In order to determine the change of resistance, values were measured between 0 and 100, after every 10 abrasions. The abrasion resistance was tested for the ink film printed on paper (Igepa Maxigloss, 135 gsm) and PET (100 µm - Melinex® 401), against similar paper and PET, as well as against a selected cloth counter piece.

Moreover, probable effects due to folding were assessed with a folding endurance test device. Thereby, the resistance was determined after every applied double fold.

As the tag layout is variable (square, octagon, circular etc.), testing was performed on the serpentine test structure, as commonly utilized for material assessment.

The effect was tested on PET (100 µm - Melinex® 401) and paper (Igepa Maxigloss, 135 gsm) with different results, depending on the substrate material. The testing setup is shown in Figure 2-12.

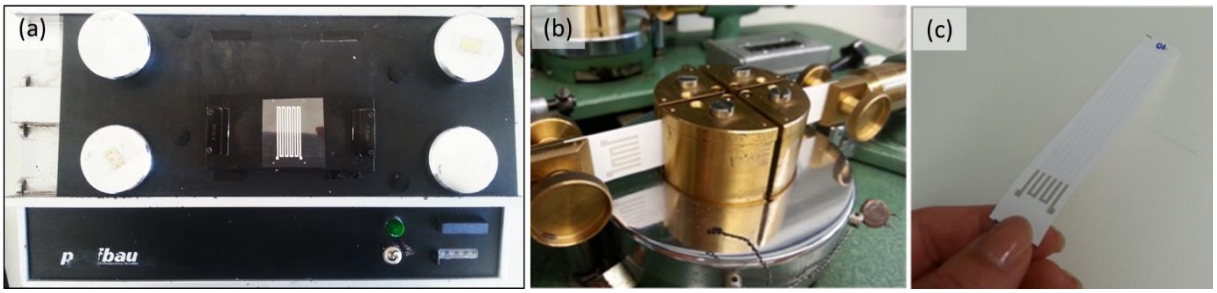

Figure 2-12. (a) tilized prüfbau Quartant abrasion tester, (b) folding endurance tester (c) test structure

The outcomes of the abrasion tests are depicted by the diagram in Figure 2-13.

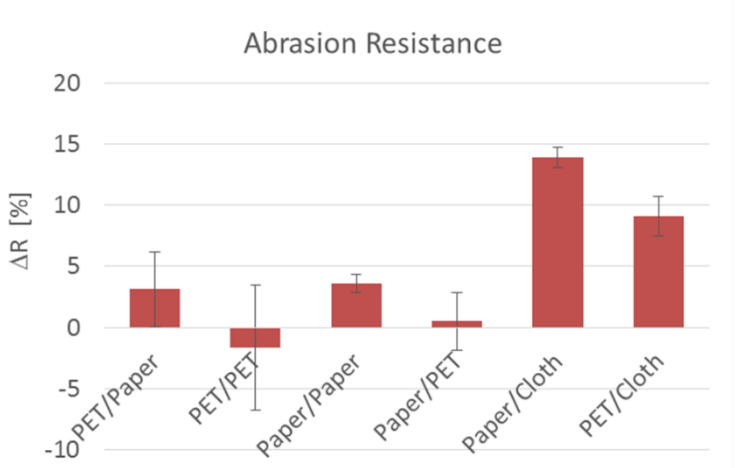

Figure 2-13. Percentage resistance change due mechanical abrasion (x-axis: printed substrate/counter piece)

It can be concluded that for all tests, a percentage decrease of resistance of less than 15% was observed after the application of 100 abrasions. While the least change of 0.5% is observed when the conductive material was printed on paper, using PET foil as abrasive counter piece, greater changes of 9.1% and 13.9% were determined for the cases where a cloth was used to test the ink's abrasion resistance on PET and paper, respectively. Therefore, it can be summarized that a tag, produced from this material **on PET and paper provides good resistance against mechanical abrasion and the drastic impairments of functionality should not be expected**. Nevertheless, the application of a protective coating can serve to entirely eliminate potential problems.

An overview of the test results of applied folding tests is given in Table 2-6.

Table 2-6. Summary of Folding Test

Substrate	Coating/ Lamination	ΔR [%]
Paper	none	∞
PET	none	73 ± 4
Paper	Coating	18 ± 1
PET	Coating	30 ± 1
Paper	Paper	330 - ∞
Paper	PET	149 - ∞
PET	Paper	10 ± 0
PET	PET	4 ± 1

From the obtained results, it is clear that the impairment of the structure is inferior on paper if compared to the observed deterioration on PET, with one exception being represented by the conductor protected by an applied coating. Nevertheless, these folding tests revealed strong changes in resistance on any of the substrate when no coating or lamination was applied. The least changes were observed for the case where the tag would be positioned insight a PET multilayer structure.

The test samples were further examined with an optical microscope Thereby, it was found that the drastic increase of resistance is strongly related to the impairment of the paper's fibers. Consequently, it is suggested that the paper should be coated with a protective film prior tag printing.

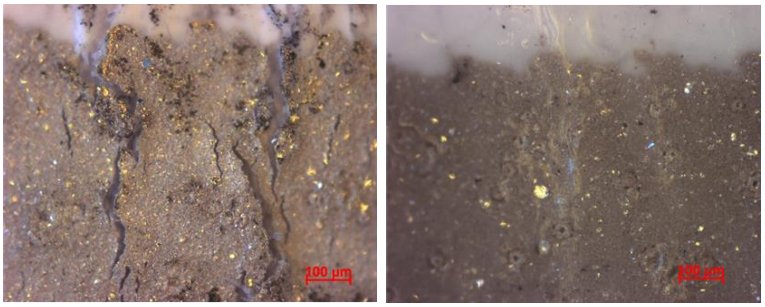

Figure 2-14. Surface of printed film after folding test: left: silver film printed on paper; right: silver film printed on paper with protective coating

2.2.1.1 Coated tags and lamination

Continuing with the considerations concerning the diversity of potential materials and taking into account the commonly applied fabrication procedures, the impact of laminations on the tag's functionality was assessed. This particularly addresses the possibility that the tags may be produced as an inlay being located inside a smart card, but also counteracts the predictable space intricacy, induced by the correlation between tag size and functionality, particularly reading range and coding capacity. In addition, coating of the tag may be advisable in order to increase scratch resistance and to avoid undesired damage due to mechanical stress. As a result of the lamination/ coating, a frequency shift is expected as the effective permittivity E_{eff} increases due to the addition of the extra layers of paper and foil. The frequency shift is predicted according to the basic formulation that relates the wavelength (λ) with the frequency (f), as follows,

$$\lambda = \frac{c}{f\sqrt{\varepsilon_{eff}}} \quad (1)$$

where c is the speed of light.

In order to clarify and confirm the absence of additional effects, for instance due to the rough surface/ interface to the tag structure or the presence of dielectric material between the single coding particles (resonators of a unitary element), laminated and coated printed octagonal chipless RFID tags were produced and assessed. In order to prevent unknown factors, the laminations were produced from known materials. Therefore, an adhesive was printed on utilized substrate materials, in particular coated paper (Igepa Maxigloss 135 g/m²) and polyester foils (100 µm PET - Melinex® 401), and combined with printed octagonal chipless RFIDs during a lamination step. The following combinations were produced:

- Substrate material: paper; laminate material: paper
- Substrate material: paper; laminate material: PET
- Substrate material: PET; laminate material: PET
- Substrate material: PET; laminate material: paper

where the substrate refers to the material, on which the tag was printed. In addition to these combinations, the thickness of the laminate was varied.

The obtained measurement results are summarized in Figure 2-15.

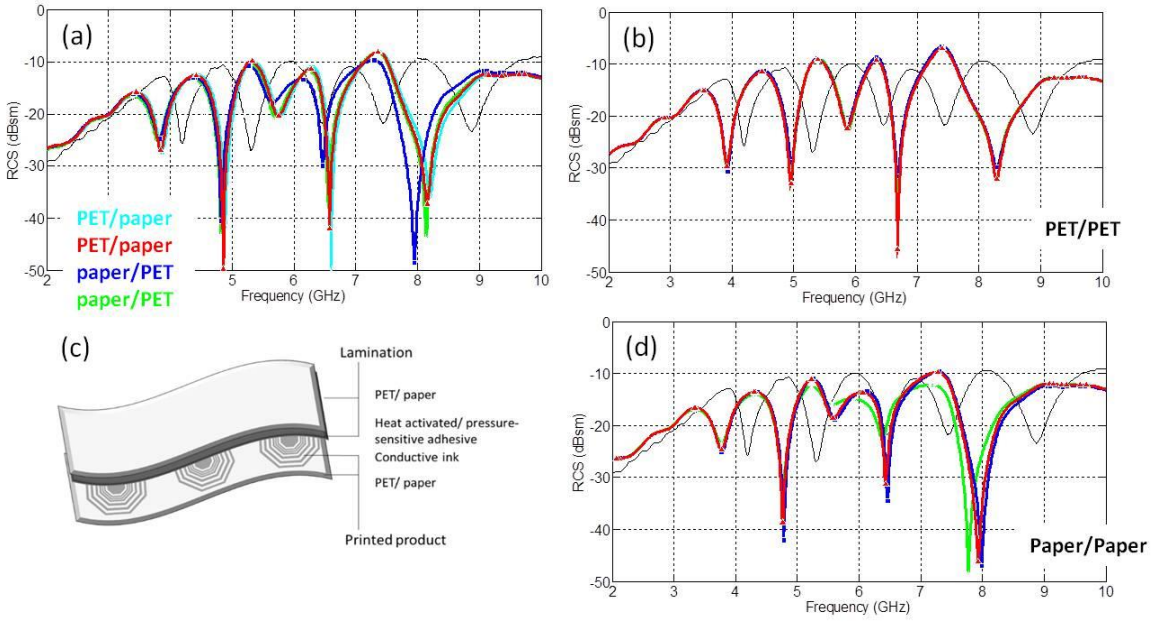

Figure 2-15. RCS of laminated octagonal tags: (a) combinations of PET and paper, (b) PET/PET (c) schematic of structure and (d) Paper/Paper

As can be seen, the expected behavior is observed. In particular, as the permittivity E_{eff} is increased by the applied paper/PET, the frequency is shifted towards lower values.

Moreover, no undesired effects are caused and all the RCS features are preserved in spite of the coating and the substrate material used to manufacture the tag.

Furthermore, just as observed for the changes of the substrate's thickness, depending on the thickness of the laminate, the peaks/notches are shifted towards lower frequencies. Thereby, the shift increases with the thickness of the laminate and is more distinct at higher frequencies.

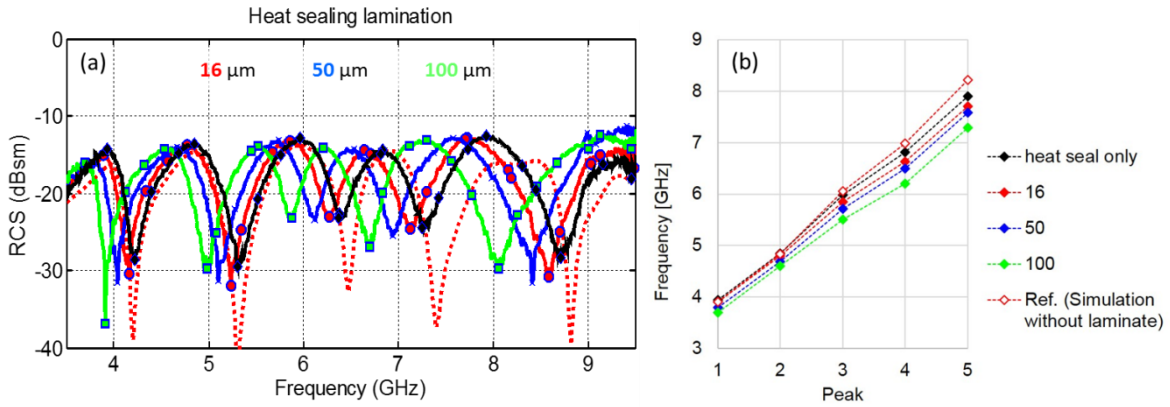

Figure 2-16. (a) RCS for 4 unitary elements and (b) peak frequencies of octagonal tags, laminated with polyester foil of various thickness

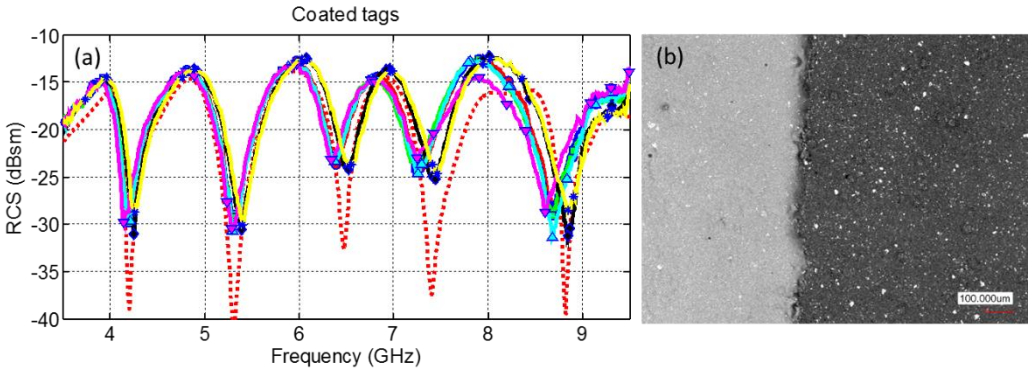

Figure 2-17. (a) RCS of coated tags and (b) microscopic image of coating

To revert the frequency signature response to the original response it could be a straightforward task to adjust the dimensions of the tag to absorb the frequency shift in advance. However, similar as concluded for the tags printed on various substrates it can be concluded that this necessity also depends on the capabilities of the reader.

2.2.2 Bending and folding effects

The objectives of this experiment are the following:

- Study the effect of the flexible substrate as the ones used to fabricate the chipless RFID tag, i.e. PET and paper
- Study of basic deformations introduced to the tag: bending and folding

This experiment is performed at the anechoic chamber in order to minimize the external RF interferences and to reduce the multipath phenomenon. The measurement setup is a bi-

static radar measurement setup. As interrogators are used two linear polarized rigged-horn antennae with average gain in the observation frequency band of 10 dBi. The measurement device is an Agilent PNA set to 0 dBm. During the measurement campaign, the measurement antennae always remain in vertical position and at a distance of about 90 cm.

The curvature and fold angle is added to the tag samples by attached them to several molds made of expanded polystyrene. This material is known to have a relative permittivity close to the unity; being perfect choice to perform far-field measurements as intended here. A picture of several tags attached to its correspondent mold are shown in Figure 2-18

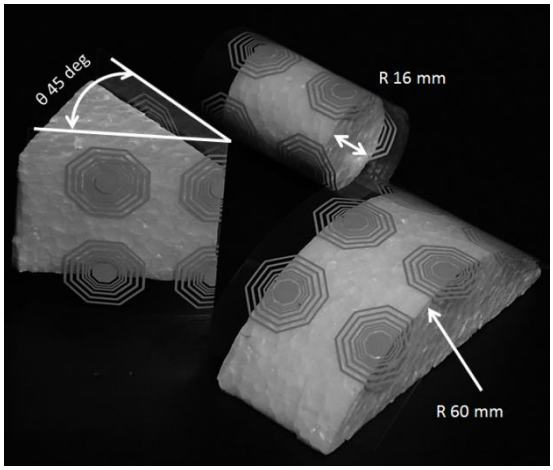

Figure 2-18. Actual aspect of some bent and folded tags mounted over its respective molds. In figure is shown the 45 deg folded tag and the 16 mm and 60 mm radii bent tags.

2.2.2.1 Bent chipless RFID tags

The measured tags include the following curvature radii: 100 mm, 80 mm, 60 mm, 30 mm and 16 mm. The measurement results are reported for two different tag positions: vertical position (V) and horizontal position (H). The horizontal position is set when the tag long side is parallel to the X axis.

From the Figure 2-19 can be observed how the performance of bent tags are affected by modifying the curvature radii; in general terms, as the bent radius decreases the lower RCS obtained from the tag. In addition to this, the good agreement between simulations and measurements for all bent radii is also observed.

It is noticeable that independently to the applied curvature, the RCS peaks and notches remain recognizable for all the reported cases. Furthermore, there is no frequency shift observed but a significant reduction on backscattered power. Therefore, it is concluded that the information stored on a bent tag can be successfully recovered.

In particular, for large radii (>60 mm, figures a and b) it is observed that the tag in H position worked better than in V position. The improvement reported in such cases is due to the light curvature and tag's axis alignment, which is better illuminated for the E-field in a V-H measurement setup. On the contrary, for lower radii (<30 mm, figures c and d), the situation changes radically and the tag in V position started to backscatter more power to the reader. For these cases, the tags in V position are better illuminated from the interrogation field and the measurement made with a V-V setup, recovers more signal strength from the tag.

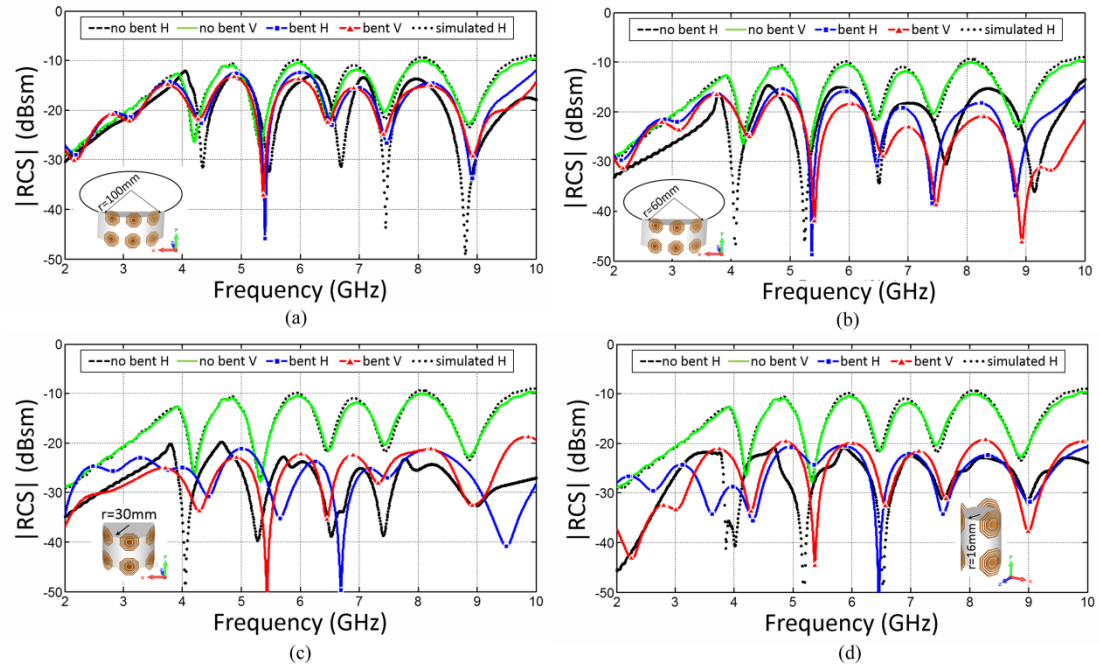

Figure 2-19. Experimental results obtained for the octagonal-shape chipless RFID tag bending with several radii, a) 100 mm; b) 60 mm; c) 30 mm and d) 16 mm. The graph includes a reference tag measured without bent and a simulation result for the tag in H position. Inset figures represent the actual curvature of the tags when are in horizontal position.

2.2.2.2 Folded chipless RFID tags

The fold angles include the following cases: 45 deg, 90 deg and 120 deg. The measurement results are reported for tags in V and H positions. The measurement setup is similar to the one used for the bent tag experiment, with the measurement antennae in V position (E-field vertically polarized).

From the results shown in Figure 2-20, it is clearly observed how the response is degraded as the fold angle is decreased from 120 to 45 deg. In comparison with the reference measurements (tag without fold in H and in V position) the response collected from the folded tag is at least 10 dBms lower. This is a direct consequence of the drastic change in the tag geometry as also was observed during the folding endurance test (see section 2.2.1)

Table 2-7.. Summary of results obtained for bending and folding effects

Summary of results
• Tags with five different bending curvatures were simulated and measured • A minimum curvature radius down to **16 mm** was experimentally demonstrated to work properly. • Three different folded structures, with different angles, were measured • A higher degradation in performance for a folded tag rather than for a bent tag is observed • The degradation in performance introduced for a bent or folded tag may lead to a reduction of the read range as well as possible bit losses.

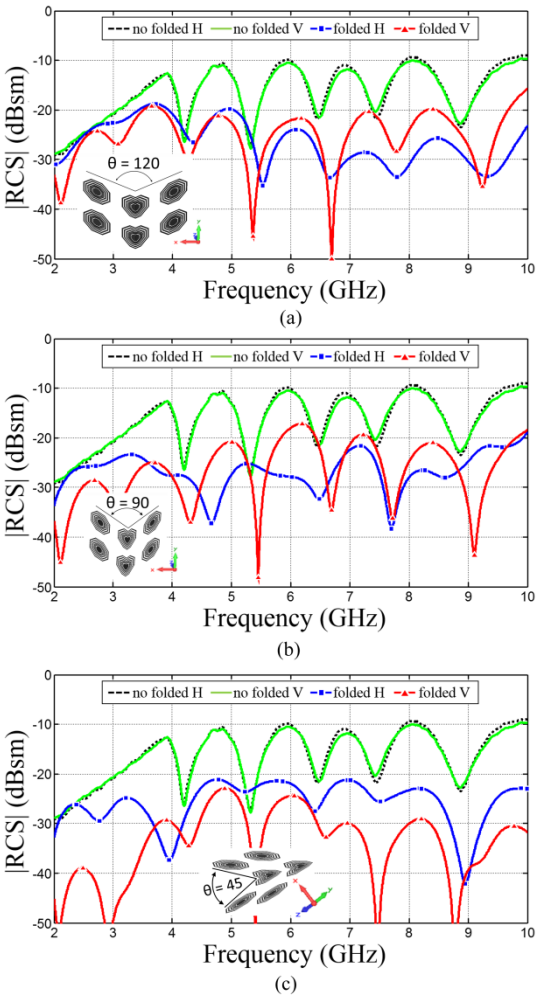

Figure 2-20. Experimental results obtained for the octagonal-shape chipless RFID tag folded to several angles: a) 120 deg; b) 90 deg and c) 45 deg. The graph includes a reference tag measured without fold. Inset figures represent the actual aspect of the folded tags. Inset on (a) and (b) are in H position and in V position on figure (c).

2.2.3 Human body effects

The aim of this task is to evaluate the effect on the performance of a chipless-RFID tag in presence of the human body. For this purpose, a chipless RFID tag held in a human-like hand is studied.

Results reported next are based only on simulation results performed on CST MWS High Frequency design tool. A simulation of the human hand model holding a tag, with a tag located in several positions, is performed. In this study, the 3D hand model included within the CST installation library is used (see Figure 2-21A). In addition to this, an alternative 3D hand model provided by DIGINEXT[2] as is shown in Figure 2-21B is used. The poses of the hand represent the most usual situations when a person holds a tag, i.e. the tag is totally covered by the hand, or the tag is gripped by the hand but the tag is not covered by it.

[2] We want to acknowledge to Mr. Romain Charbit from DIGINEXT for providing us with this specific model

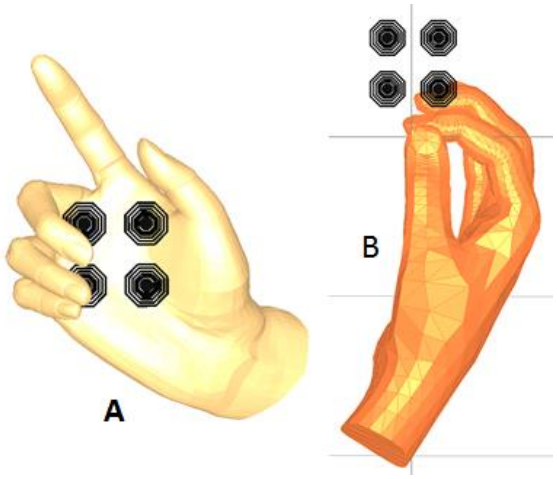

Figure 2-21. Human hand models used in this study. A. CST model and B. DiGINEXT model

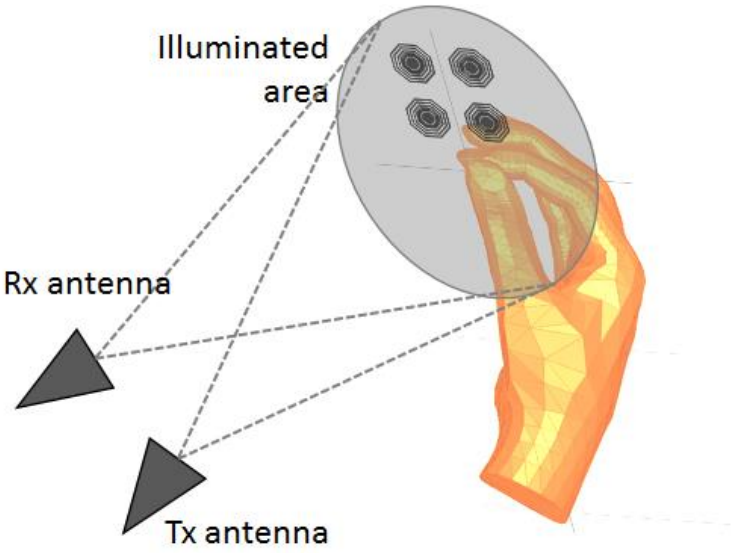

Figure 2-22. A hand holding a tag. In this case, the interrogation signal impinges the set hand-tag

The simulation setup is as the one illustrated in Figure 2-22. In this setup is included a hand model and an octagonal tag. The illuminated area represents the spot-beam as launched per the Tx antenna. The following table summarizes the results obtained in this experiment according to the position of the spot-beam (illuminated area).

Some conclusions can be driven from this study, as follows:

- The results obtained in simulations and from some initial experiments suggested that **the human body, i.e. a hand, body torso, etc, represent a significant obstacle to the radar phenomenon to work as is ideally expected**. This specially applies to simplified reader setups as are the reader test-beds developed for eVACUATE project.
- Simulation results also suggest the necessity to avoid the obstruction of the line-of-sight between the reader and the tag. In all cases where the tag is blocked or in the presence of a surrounding element, the information from the tag is strongly deteriorated. Nevertheless, the information from a tag, when it is held on a hand,

can be recovered provided that the interrogation signal only illuminates the tag but not the set tag plus hand.

- In order to avoid or reduce the human body interference on chipless RFID tags, a set of **recommendations** must be followed, to know:
  - Tag should not be covered by any part of the human body in order to be identified.
  - Tag must be not carried in pockets
  - Individuals have to be willing to present the Tag to the reader
- Obtained results are not conclusive and further research work in this area to dismiss the impact of the human body in the performance of the chipless RFID tags has to be done. Other analysis alternatives as e.g. a pure time-domain methodology must be explored. On the other hand, the evaluation of alternative working frequency bands, with low interaction with human body tissues, must be considered.

Table 2-8. Summary of results obtained for human body interference

setup	Description	Results
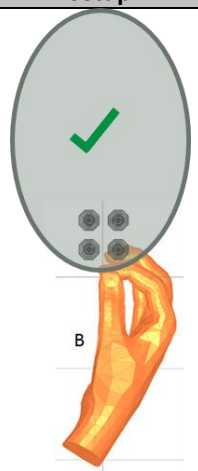	• The tag is gripped by the hand • The hand is not touching any part of the tag • The spot-beam only covers the tag but not the hand	Information from tag can be read
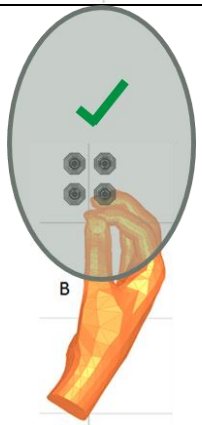	• The tag is gripped by the hand • The hand is not touching any part of the tag • The spot-beam covers both the tag and a small portion of the hand	Information from tag can be read
	• The tag is gripped by the hand • The hand is not touching any part of the tag • The spot-beam covers both the tag and the complete hand	Information from tag cannot be read

	• The tag is on the hand's palm and the spot-beam covers both the hand and the tag. • The hand is touching the tag	Information from tag cannot be read

2.3 Cost of octagonal and circular tags

For the estimation of the tag cost, the most convenient scenario, where the tag is directly printed on the end-user substrate was considered, as it is associated with the least costs incurred. In particular, additional substrate costs are eliminated and due to the application of a high-throughput mass printing technology, the cost fraction to be taken into account for the additional production step is comparably low (as compared to conventional manufacturing methods). Therefore, **the ink can be considered as the main driver for the tag cost**. During gravimetric measurements concerning the applied transfer process and materials used to prepare octagonal and circular tag versions, an average ink transfer of 3.67 mg/cm² was determined. This relates to a minimum ink consumption of 35.18 mg/tag and 22.97 mg/tag for octagonal and circular (version 2) tag versions, which equates to expected **material costs of 3.34 €-Cent/tag (~27 cm²/tag)and 2.15 €-Cent/tag (~29 cm²/tag) respectively**. These values are based on an ink price of 950 €/kg[3]. As the price is controlled by the silver cost and respective reductions of the purchase price cannot be presumed with certainty, it is clear that the initial **price objective (< 1 €-Cent/30 cm²), is not achieved**, as the targeted value is already exceeded by the ink cost only, not taking into account the additional labor, machine and material costs (printing screen etc.).Therefore, adequate replacements and alternative approaches were reviewed and analyzed.

An obvious approach consists in the reduction of ink consumption, which implicates the need for a range of considerations as the functionality is directly affected by either reducing the thickness, the printed area or both. As the requirements on the chip-less RFID technology, particularly the minimum reading range of 1m, utilization of flexible low-cost substrates and the demanded independence to the polarization, have been leading to a design with particularly high utilization of surface area, the reduction in terms of a decreased amount of unitary elements cannot be commensurate. Another potential approach to decrease the ink consumption does further consist in the replacement of larger solid areas by a grid structure as for instance assessed for UHF antennas in ref. [Sid05]. However, if applying the approach to the inner solid area of the octagonal elements, a sufficient decrease cannot be achieved, particularly, with the solid area accounting for approximately 15% of the total area.

Furthermore, it was found that the thickness of the ink film needs to be significantly reduced in order to reach below 1 €-Cent. In fact, a theoretical dry-film thickness of less than 1.5 µm (octagonal tag/ 4 unitary elements) was estimated. This is rather problematic, as this film thickness is not realizable by the applied printing technique and micro-particle based silver ink. Results obtained with other technologies further suggest that the reduction of the dry film thickness below this limit value involves the reduction of conductivity to dimensions where severe functionality degradation is observed as a consequence of apparent conductor losses. Therefore, **the reduction of the conductor's thickness was identified as inapplicable approach**. Applying the similar estimation to the circular tag version, a dry film thickness of less than 2.4 µm is considered for the ink price to fall below 1€-Cent. However, a study performed on the initial circular tag version reveals the expectable consequences. As pointed out with the help of Figure 2-23, the conductivity of the structure decreases as the

[3] price list provided by DuPont for a Kg of conductor paste with Ref. 5028 in 2015

layer thickness is reduced. As a consequence, the dynamic margin (difference between peak and notch) decreases. In the case, where the thickness was reduced to about 1.4 µm, the specific conductivity drastically reduced to 2,250 ± 95 S/cm. The designed response in terms of expected peaks and notches were not retrieved or said differently, the dynamic margin was reduced to zero. This can be associated to the increased conductor loss, as a result of lower conductivity and decreased thickness. Moreover, it has to be taken into account that this tag design is composed of resonators with a width of 1 mm. Considering the dimensions of the circular tag version 2, the resonator widths range from 0.3 to 1.1 mm. Taking into account the reduction of the structure's conductivity with respect to decreased resonator widths, the reduction of the thickness below the determined limit value of 2.4 µm cannot be recommended.

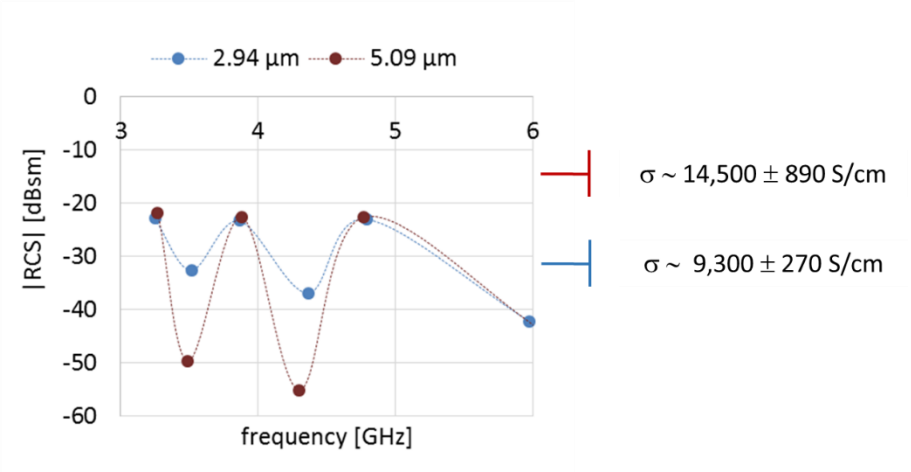

Figure 2-23. Effect of conductor thickness reduction on the radar cross section

To counter the potential situation, in which the tag's advantages might be subordinated to the cost, alternative and potentially less costly materials would be desirable. During an earlier stage of the project, two classes of innovative materials from the research field 'Printed Electronics' have been already assessed with regard to their capabilities for the production of resonating structures to form chip-less RFID tags, in agreement with the requirements, determined by the eVACUATE system. It was concluded that both, carbon-based inks and conductive polymers, do not possess the required characteristics necessary to provide the desired functionality to the chip-less RFID tags for eVACUATE project.

Consequently, the review of potential materials was extended to alternatives even beyond the commonly adopted particulate inks and dispersions.

2.4 Alternatives

Within the framework of the development task, a range of materials were tested and assessed with regard to their suitability for the production of chipless RFID tags that comply with the specified system requirements.

Due to the comparably low conductivity, innovative printed electronics materials like conductive polymers had to be excluded for the production of chipless tags. A few more elaborated tests were conducted with carbon-based materials (see deliverables D7.1 and D7.3). However, the probable potential of the materials, as for instance described in [Hua15], could not be exploited, as herein utilized, commercially available inks could not provide sufficient conductivity. Consequently, the material was excluded for further developments for the eVACUATE chipless RFID system.

2.4.1 Copper ink tags

Despite the before mentioned, inks based on conductive copper flakes were considered for tag production. Three roll-printable inks were selected to prepare test samples by screen printing and flexography on both, paper and PET substrates. An overview is given in Table 2-9.

Table 2-9. Characteristics of utilized Copper Inks [ELA_]

Ink	Pigment Content	Total Ag Content	Pigment Size	Viscosity	Printing
1	N/A	70 ± 2%	1.0 ± 0.2 µm	20,000 ± 1000 mPa·s	Screen
2	40 ± 2 %	10 ± 2 %	4.5 ± 1.0 µm	~270 mPa·s	Flexo/ Gravure
3	50 ± 2 %	20 ± 2 %	4.5 ± 1.0 µm	~400 mPa·s	Flexo/ Gravure

Based on the results of initial printing tests, copper ink 2 and 3 were used to prepare further test samples with various layer thicknesses and thus films with different sheet resistance.

After evaluation, circular and octagonal tags were printed to assess the radar cross section and estimate the capability of the material for tag production. The tags were prepared at the test printing device Flexiproof 100 (Erichsen) with a printing speed of 0.67 m/s and dried at 80°C (see deliverable D7.1 for further information on printing setup and settings adjustment).The measurement results obtained from octagonal tags on 100 µm thick PET substrate are summarized in Figure 2-24. The results of tags with 3 different layer thicknesses of copper ink 3 are shown. The tags work well until 6 GHz, but deviate from the expected behavior at higher frequencies. After further analysis of the printed structures, it was suggested that typical defects that are associated to the applied printing technology, such as viscous fingering (see height images in Figure 2-25) and squeezed edges and corresponding gain (increase of structure width) as depicted in Figure 2-24 (d) and (e), might have caused the observed phenomenon.

As a consequence, the use of this material was suggested for tag designs with lower frequencies, e.g. circular tags (see deliverable D7.3 for tag design). A summary of obtained results for the circular tags on PET samples can be found in Figure 2-25.

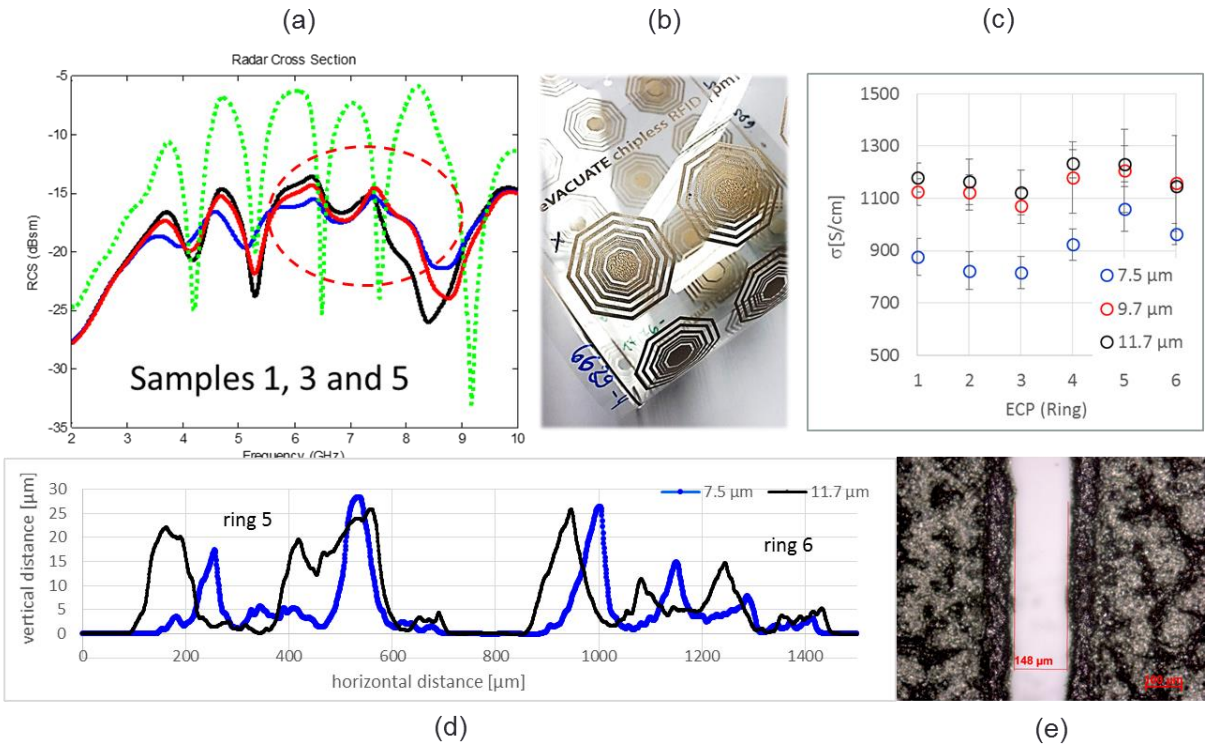

Figure 2-24. (a) Radar Cross-Section, (b) photograph, (c) single resonator conductivity, (d) profile of inner resonators, (e) microscopic image of octagonal-shape tags printed with ink based on copper flakes (Copper Ink 3)

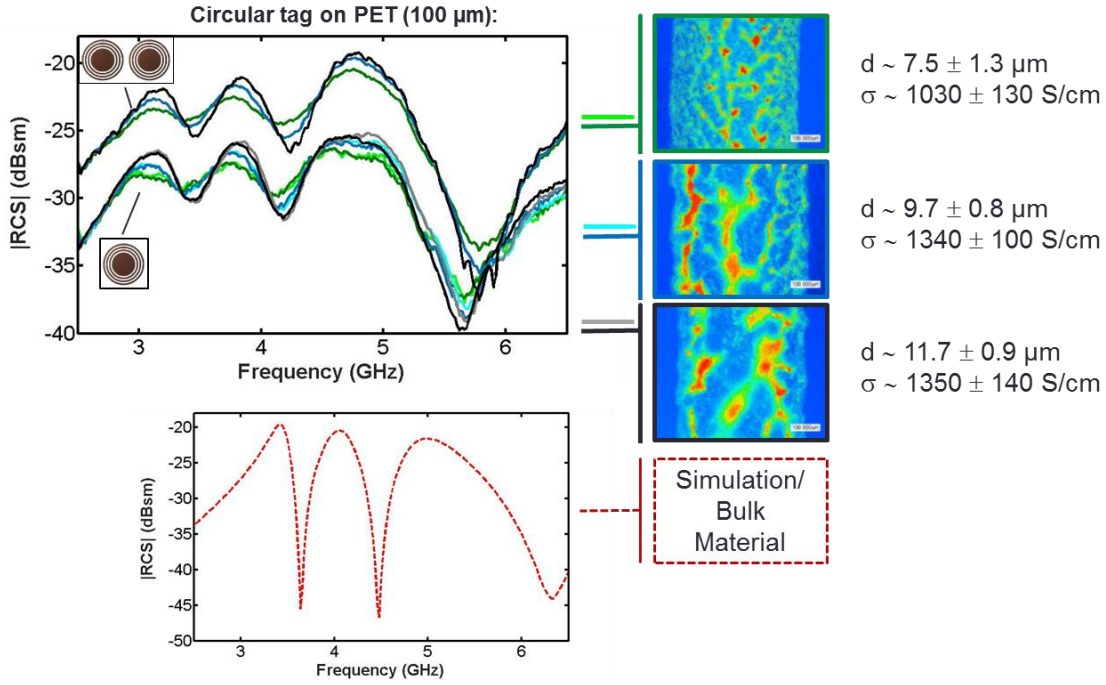

Figure 2-25. Characteristics of circular tags fabricated from water-based ink containing copper flakes (Copper Ink 3)

As can be seen, the engineered frequency signature of the circular tag design can be retrieved and therefore, the tags can be considered as functional for both, the one period and two periods' cases. It is further visible that enhancements in the shape of the radar cross section's magnitude are achieved as the ink's effective area is increased. However,

even if the dynamic margin slightly improves as the conductivity increases, as a consequence of the comparable low conductivity of the produced films, it still remains rather low as compared to silver ink tags, where the dynamic margin accounted for approximately 30 dBms, which is almost 20 dBms lower for copper ink tags with highest thickness and conductivity. This reduces the robustness of the system as reading errors may occur.

Moreover, if considering expected ink cost reductions being the main driver for testing the alternative materials, the achievement of this targeted decrease was evaluated with respective gravimetric measurements in an analogous manner as for silver ink tags with the following results. In order to produce dry films with thicknesses of 7.5 µm, 9.7 µm and 11.7 µm, 2.5 mg/cm², 3.8 mg/cm² and 4.5 mg/cm² conductive ink have to be deposited. With a purchase cost of 500 €/kg, ink for one period of the initial circular tag design would account for 0.52 €-Cent, 0.79 €-Cent and 0.94 €-Cent respectively, reducing the ink cost from initial 1.46 €-Cent for the printable silver conductor by up to 64 %. However, considering the need to include several periods in order to provide sufficient robustness and reading range, **the use of the material for eVACUATE chipless RFID production is not suggested**.

2.4.2 Foil tags

One of the critical factors for the printed conductors performance is the conductor loss, which is usually due to the application of printed electronics materials and processes that introduce imperfections to the conductive material, e.g. due to the way the conductor particles form electrical contact, presence of air inclusions or comparably high roughness (as compared to bulk material). Therefore, materials with properties more similar to bulk materials that still allow the application of high throughput processing technologies are desirable.

Hence, this work was extended to the study of some possible alternatives that are known from printing industry, as well as from conventional microelectronics. Especially, the options from the printing industry seem rather appealing as the applicability of high process speeds is known, fabrication steps may be easily integrated into production and lower costs are expected.

The structure of the utilized metallized films provide properties comparable to bulk materials, but are usually characterized by very low film thickness in the nano-meter range. Therefore, the influence of skin effect on the performance of the tag has to be taken into account. Especially, for thin structures like tested metallized films, increased loss should be expected for frequencies that correspond to or even fall below skin depths that are close to the printed conductor thickness. As the latter is usually notified by the increased bandwidth of the input impedance (as an effect of the increased loss of the conductor) [Man09], tags with designs as presented in 2.1.1 and 2.1.2 may not be realizable.

Whether and to which extent these materials may fit the chipless RFID technology requirements and can be applied for their production, has been studied herein.

The review of existing technologies and available materials resulted in the suggestion of two possible approaches to form the conductive pattern. Both are relying on the subtractive generation of the structure, but differences occur with regard to the pattern fabrication and

the composition of the films, which further entails differences with regard to the electrical conductivity, layer thickness, edge sharpness and resolution. The considered technologies to pattern the metalized film are categorized into etching methods and foil transfer procedures. The first type origins from conventional micro-electronics and may be described as an up-scaled manufacturing process, suitable for roll-to-roll production of printed electronics devices. Common etching procedures include the application of an etch mask/ etch resist, which is followed by etching off the unexposed areas. In order to keep the complexity of the production low, a procedure with a minimum of process steps is desirable. Hence, a direct etching procedure is preferable. This kind of procedure has for instance been reported for the production of piezoelectric energy harvesting devices as reported in [Ali14] and was adopted herein for test sample preparation in order to estimate the potential applicability of a zinc metalized film. Differently as reported in [Ali14], screen printing was applied for etchant deposition as high resolution and good edge sharpness was required.

The second manufacturing approach was used to test the suitability of aluminum metallization for the fabrication of chipless RFID tags. The method origins from commercial printing and is often applied in packaging, where it is used to create visual effects on the printed product. Two major transfer technologies can be distinguished; hot foil stamping and cold foil transfer. Both principles have been rarely considered for the use in printed electronics and only view indications about their suitability can be found in the literature as for example in [Lya14]. Generally, the latter technique would be preferably, since it is attributed to lower fabrication costs.

Herein, a range of both, hot foil and cold foil printing materials, as well as etched metallization, have been assessed with regard to the processability and sheet resistance. The outcomes of the tests are summarized in Table 2-10.

Table 2-10. Summary of Test Results on Metalized Films

Foil type	Sheet Resistance [Ω/sq.]	Printability/ Processability
Zinc metallized film	~ 8.5	R2R-Etching/ good
Zinc-Aluminum metalized films	> 0.9	R2R-Etching/ poor
Aluminum metallized films	> 1.5	R2R-Foil Transfer/ very good

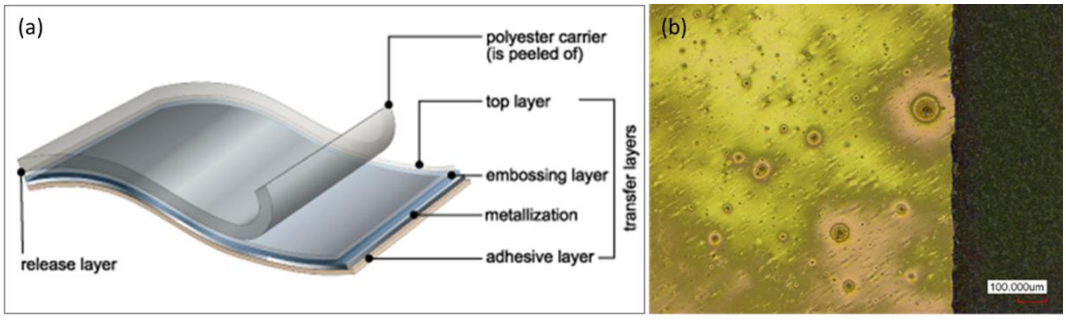

Figure 2-26. (a) structure of hot stamping foil [Kur15], (b) microscopic image showing edge of transferred film

Even though the lowest sheet resistance was obtained for one of the tested zinc-aluminum metalized films, the poor processability of the material resulted in its elimination for further

work. Considering the commercially available hot and cold foiling materials, the lowest sheet resistance was determined for one of the hot foiling materials and did account for 1.51 ± 0.06 Ω/square, which is in the range of copper samples with lower thickness. As the material further provided good printability, the material was selected for further testing. A simple foil fusing test bed was utilized to prepare a range of test layouts. The simple procedure includes two steps. During a first step, the printing image is produced with a hot melt glue and during the second step, the printed image and foil are combined in a lamination step. Herein, black toner was printed in a Xerox 770 Digital Color Press by Xerography (direct dry toner transfer), followed by a lamination step, utilizing a simple SKY-DSB laminating device (Model SKY 480R6) set to 120°C and a lamination speed of 8.7 mm/s. A sample for a foil-tag is described in section 2.4.3.1.

2.4.3 High capacity tags

For a market ready devise based on chipless RFID technology it is desirable to count with a high capacity tag, i.e. higher than 3 bits as per DoW required. For this purpose, one of the tasks agreed between the Project coordinator, the Work package leader and the technical partners (TUD and TUC) to be performed in the last period of WP7 was to try to increment the capacity of the chipless RFID tag.

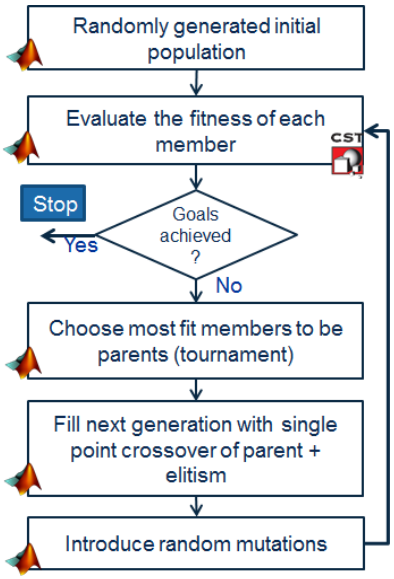

Figure 2-27. Flowchart outlining the evolutionary process of a GA.

The solution proposed is named as "Genetic Algorithm based tags –GA_tags". Those tags can codify (theoretically) between **8 and 14 bits**. First demonstrators for this novel technology has been fabricated by TUC and measured by TUD showing the viability of the proposed design.

2.4.3.1 GA based tags

The Genetic Algorithm is a widely known robust optimization technique which searches in a large parameter space for a solution that simultaneously meets multiple design criteria [Boss06]. Operating based on the principles of natural selection, GA mimic the evolutionary process, where a population of possible designs is iteratively mated, weeding out poorly

performing members of the population, while retaining only the best performing members, until a design that meets the specific requirements is ultimately found.

A flowchart outlining the operation of the GA used to design chipless RFID tags is shown in Figure 2-27. An initial population of binary chromosomes is randomly generated, and each member of this population is evaluated using CST to compare its RCS response with a specified RCS response. Once the entire population is evaluated for fitness, the population members are ranked, and tournament selection is used to choose parent for the next generation, i.e. the best responses are chosen. The selected parents are mated to generate child population members. Random mutations are introduced into the population, and the best response from last generation is kept for the new generation. This iterative process is continued until the GA converges to a solution that meets the specified design criteria. The control of the process is made using a Matlab routine which also controls the CST simulation software.

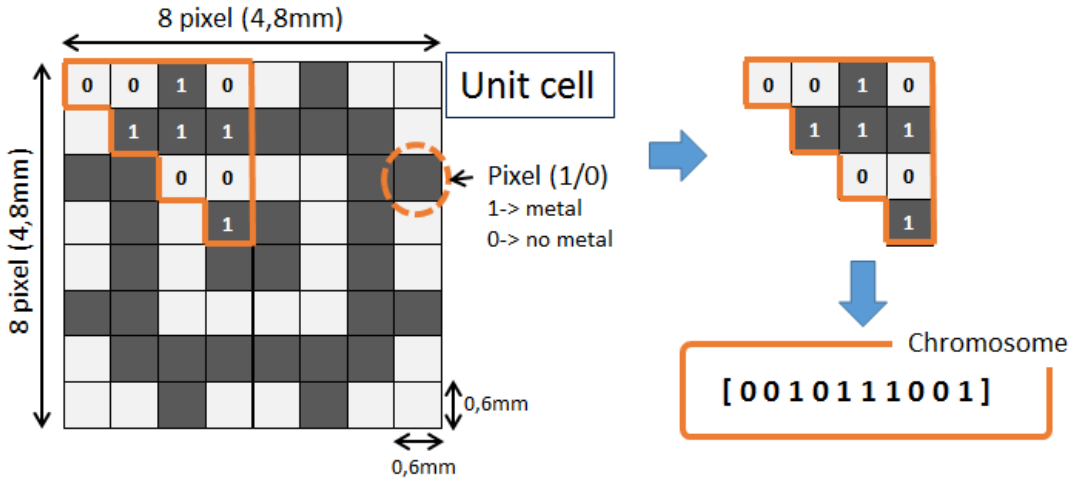

Figure 2-28. Unit cell of a GA based chipless RFID tag with chromosome pixel values.

Because the substrate and dielectric characteristics for the tag design were chosen a priori, the only parameter represented the chromosome were the metallic screen geometry and the unit cell size. The unit cell size can be comprised by several pixel size grids, to know: 60 x 60 pixel, and 32 x 32 pixel.

The binary values indicate the presence (“1”) or absence (“0”) of metal in a given pixel. Eight-fold symmetry is applied to the unit cell to achieve polarization independence. Thus, only one triangular fold of the unit cell is encoded into the chromosome (see Figure 2-28). The pixel size is constrained to be larger to the minimum resolution of the screen method used to fabricate the tags.

The fitness of each candidate design is measured against a desired RCS response. Several pass-band and stop-band frequencies are chosen over the desired band operation (UWB). Then, each design is simulated at specified frequencies and penalized for energy transmitted at stop-band frequencies and energy reflected at pass-band frequencies.

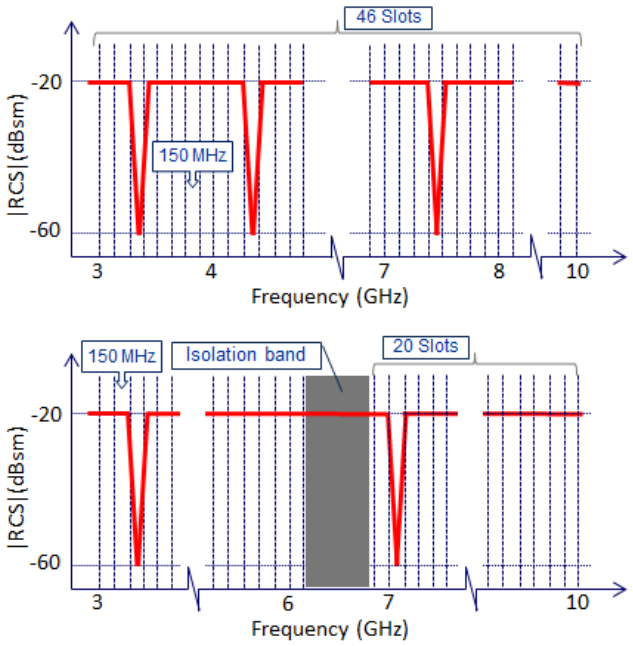

Figure 2-29. Frequency Shift encoding technique applied to the GA based tag design. Above, the UWB are divided in 46 slots of 150 MHz each to obtain a tag capacity of 14 bits by using 3 resonances. Below, the division of the UWB in two sub bands of 20 slots each to codify up to 8.6 bits by using two resonances.

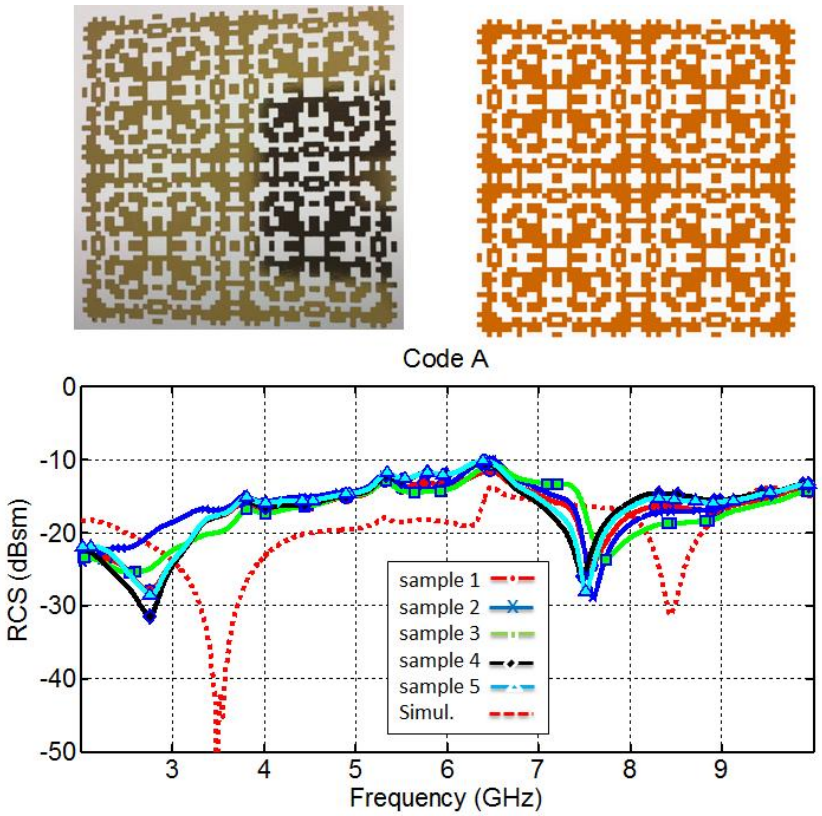

Figure 2-30. CAD design, fabricated sample, and measurement results obtained from a GA based chipless RFID tag with two resonances.

The coding technique applied to the GA based tags is the frequency shift encoding [Ven12]. To implement this technique, the frequency band is divided in several frequency slots, each

one of ~150 MHz wide. So we get ~46 slots as is shown in Figure 2-29. By using tags with 2 resonances (notches) located in different slots, it is possible to have up to 1035 different options, or what is the same, a capacity of 10 bits. When 3 resonances are chosen, the possibilities can grow to 15180, meaning a capacity near to 14 bits. For the correct implementation of this technique, we assume that the GA is able to allocate a resonance (dip) in each of the slot selected to be used to codify the tag (usually 2 or 3 dips are necessary). Additionally, some restrictions apply to the tag design in order to achieve such high (theoretical) capacity, for instance the necessity to separate two neighbor resonances by a minimum space in frequency (larger than actual slot wide), in this case, a division in the available slots could be applied and separation slots in between can be defined. In this case by choosing two frequency bands of 20 slots with a separation of 6 slots in between, can lead us a capacity of 400 options or 8.6 bits.

The first GA tags fabricated using flexible substrates are shown in the Figure 2-30. Those tags were fabricated at PM-TUC using the design techniques explained in section 2.4.2. From the results obtained and shown in same figure, several conclusions arise, as follows:

- The results demonstrate that fabrication of tag based on genetic algorithm is feasible.
- The measurements results are shifted to lower frequencies due to the use of paper as a substrate in the fabrication process. The simulations were done using a different material.
- The measurements do not match with the finite size simulated tag. On the results a loss on the quality of the resonances (notches) is clearly observed. For codification purposes, those dips are of vital importance to avoid misinterpretations of tag code. This is mainly due to the lack of definition of the real material use on fabrication in the CAD software.

3 Chipless RFID reader

Since both readers hardware's descriptions were already provided in D 7.3, this chapter is based in the development of the decoding techniques as well as the presentation of the graphical user interface of the reader's consoles and reading results. The actual aspect of both readers, Novelda radar-based and the UWB Frequency based is shown in Fig. 3.1.

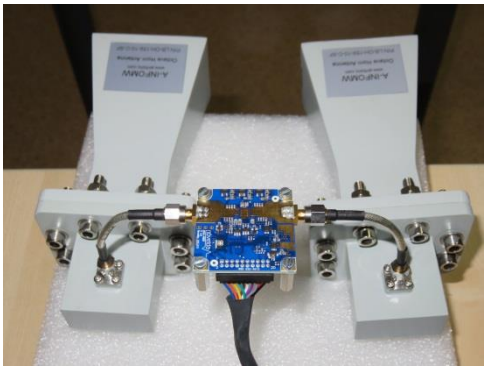

(a)

(b)

Figure 3-1 Actual aspect of reader test-beds, (a) Novelda radar-based, and (b) UWB Frequency based.

3.1 Decoding Techniques

The decoding is the part of the process where the information stored in the received signal is retrieved. To achieve this purpose, a detection algorithm must be implemented and in order to do this, certain detection must be defined. These conditions are depicted in Figure 3-2 and are meant to test the decoding algorithms on the two set of fabricated tags. In Figure 3-2, the rows represent the measurement results of the correspondent tags set used, and the columns the specific evaluated condition, which are: (a) Received signal without noise and pathloss[4] contributions, where each of codes is clearly visible to the human eye, (b) Received signal without noise contributions but including the pathloss, and (c) Received signal embedded in noise and with pathloss contributions, this last one representing a real case scenario where the signal detection should take place.

In the first two test scenarios, some previous processing is required by characterizing the noise and the pathloss in order to be able to obtain an almost noise free signal representation, for both cases each code can be clearly distinguished from the others by the human eye. And as mentioned, Figure 3-2c represents the real case where the signal is embedded in noise, therefore making it difficult to differentiate one code from another. This is where the effectiveness of the detection code and the coding technique should be tested. To perform this, three different detection algorithms are introduced in the following sections: Detection based on Power Peaks, on Correlation and on Maximum Likelihood.

[4] **Pathloss** (or path attenuation) is the reduction in power density (attenuation) of an electromagnetic wave as it propagates through space. **Pathloss** is a major component in the analysis and design of the link budget of a telecommunication system.

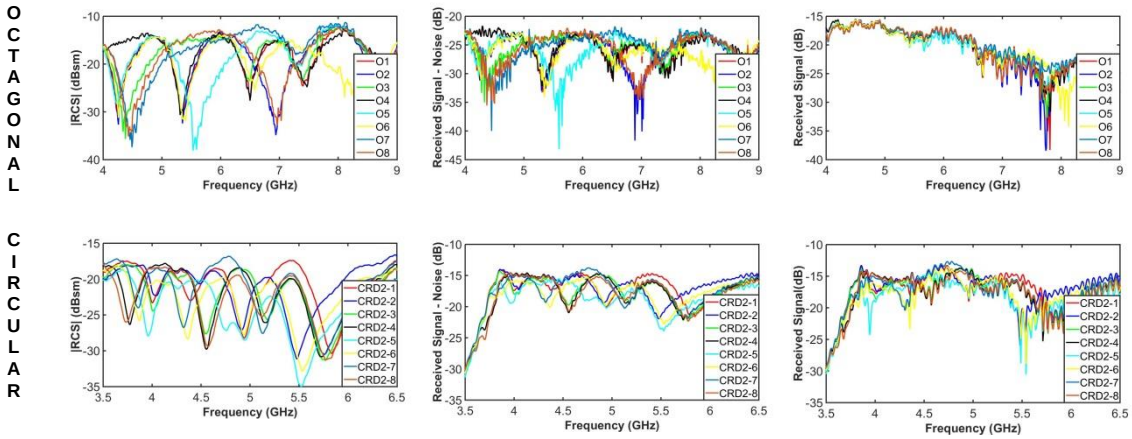

Figure 3-2. Receive Signal of Octagonals and Circular Tags depicted in rows 1 and 2 respectively. The colums represent (a) Noise and pathloss free signal, (b) Noise fee signal, and (c) Received signal

3.2 Detection by means of power peaks

The first detection algorithm implemented is based merely on a peak detector, since each tag code is characterized by its peaks and dips on specific frequencies. As shown in Figure 3-3., the algorithm searches in the places where the peaks and dips of a specific frequency shift coded tag should be. Then by means of equation 3.1, an averaging of 10 points is performed on these regions to improve the detection by reducing the influence of noisy samples and finally the decision rule shown in equation 3.2 is applied to identify the respective tag.

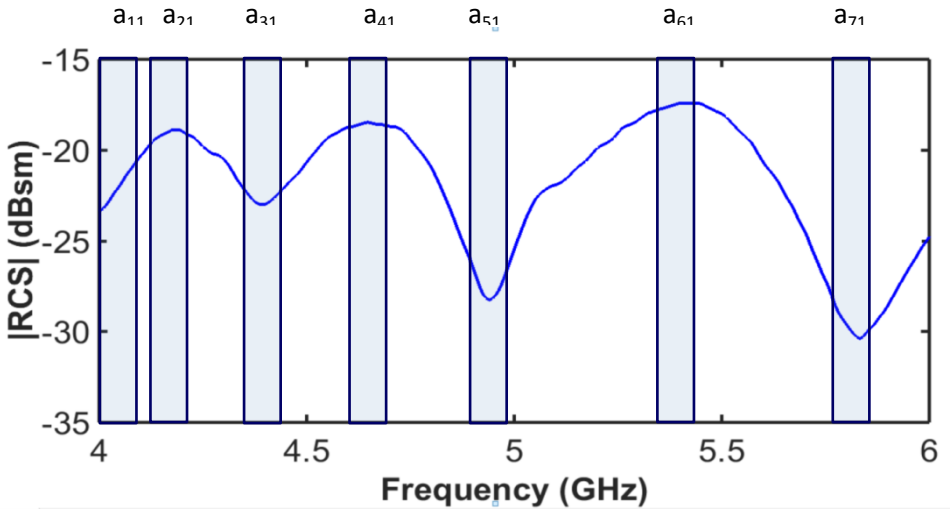

Figure 3-3. Decoding technique using the peaks and dips

$$a_n = \frac{\sum_{m=f}^{f+10} |RCS(m)|}{10} \tag{3.1}$$

$$if\left(\text{and}\big((a_1 < a_2 > a_3), (a_3 < a_4 > a_5), (a_5 < a_6 > a_7)\big)\right) \tag{3.2}$$

The drawback of this algorithm is that a pre-processing of the signal is required, namely the characterization of the path loss and the noise, in order to obtain a clear differentiation

between peaks and dips making this algorithm quite challenging to be implemented in a real scenario. Furthermore, its reliability is reduced by using only a few points of the whole scanned frequency spectrum, therefore disregarding valuable information that could improve the robustness of the detection.

3.2.1 Detection by means of Correlation

The second algorithm explored uses the correlation between the received signal and the whole set of stored originals following eq. 3.3. This technique helps to provide a measure of how similar two signals are; a block diagram of the detector is shown in Figure 3-4. As shown, after the correlation is performed, the detector selects the value with the higher correlation as the code that was received.

$$Corr_{s,r} = \int_{-\infty}^{\infty} s(u + \tau) r(u) du \tag{3.3}$$

where

$r = s + n$; r is the received signal; $s$is the transmitted signal; and n represents the receiver's noise.

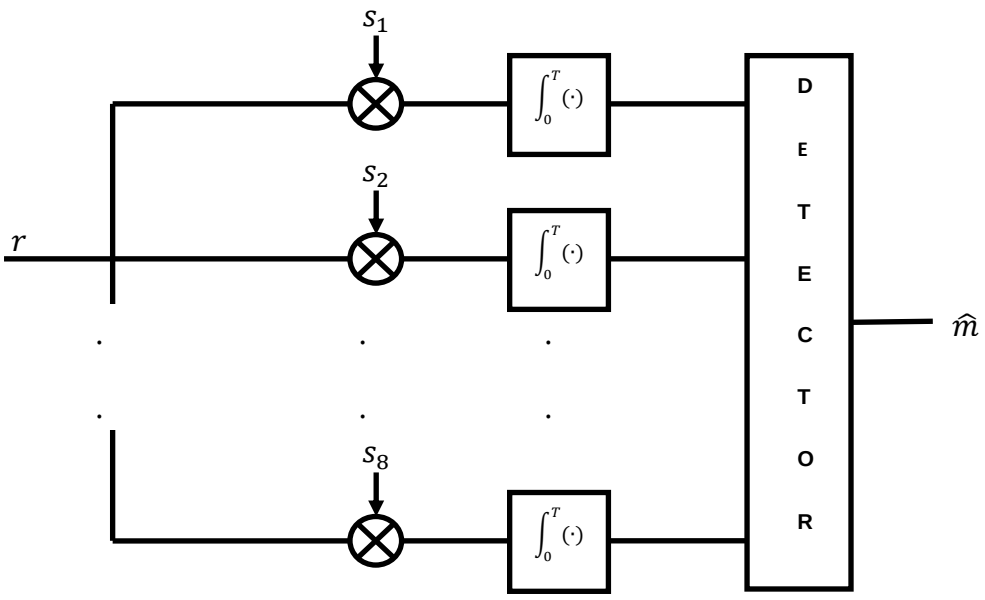

Figure 3-4. Block diagram of the correlator detector

Table 3-1 shows the correlation results between each type of tag and each stored code in a noise and pathloss free scenario. The one with the higher correlation are marked in bold and is also the one given as received code. As can be seen, the Octagonal tags are completely decoded under these circumstances and only 5 codes of the circular ones are successfully decoded, as expected codes 2 and 5, as well as 4 and 8 are confused with each other given the similarities between them as explained in section 2.1.2

Table 3-1. Correlation results for noise and pathloss free signals

Tag Type	Received Signal	Tag 1	Tag 2	Tag 3	Tag 4	Tag 5	Tag 6	Tag 7	Tag 8
OCTAGONAL	Tag 1	**0.7118**	0.6586	0.4824	0.6269	0.5475	0.5078	0.4381	0.4977
	Tag 2	0.6585	**0.836**	0.5609	0.5661	0.5256	0.4084	0.565	0.5989
	Tag 3	0.4823	0.5608	**0.7449**	0.3889	0.5061	0.3142	0.5318	0.6842
	Tag 4	0.6269	0.5662	0.3889	**0.7317**	0.4686	0.48	0.4209	0.4214
	Tag 5	0.5476	0.5255	0.5061	0.4686	**0.8958**	0.3212	0.753	0.4561
	Tag 6	0.5079	0.4086	0.3142	0.4801	0.3212	**0.6171**	0.3459	0.3779
	Tag 7	0.0438	0.0565	0.0532	0.0421	0.0753	0.0346	**0.1052**	0.0585
	Tag 8	0.4976	0.5989	0.6843	0.4213	0.4561	0.3779	0.5852	**0.8766**
CIRCULAR	Tag 1	**0.3923**	0.2469	0.2483	0.1893	0.1853	0.1953	0.2743	0.2109
	Tag 2	0.2469	**0.3465**	0.2082	0.1529	0.2335	0.1942	0.169	0.1596
	Tag 3	0.2482	0.2081	**0.3291**	0.2565	0.1715	0.1443	0.2322	0.2419
	Tag 4	0.1892	0.153	0.2566	**0.3465**	0.1248	0.1607	0.2569	0.3266
	Tag 5	0.1852	**0.2335**	0.1716	0.1247	0.2265	0.1342	0.1145	0.1176
	Tag 6	0.1953	0.1942	0.1444	0.1606	0.1342	0.2348	**0.2353**	0.153
	Tag 7	0.2742	0.1691	0.2321	0.2569	0.1145	0.2353	**0.3932**	0.2335
	Tag 8	0.2107	0.1596	0.2418	**0.3265**	0.1176	0.1532	0.2335	0.3204

Table 3-2 shows the correlation results in a noise free scenario but with pathloss contributions. As well as for the noise and pathloss free case, all Octagonal tags are correctly decoded but the amount of successfully detected codes for the circular tag is reduced only to 2. And finally, Table 3-3 shows the result for the real case scenario, for which only one of the codes is detected successfully for both types of tags.

Table 3-2. Correlation results for noise free signals

Tag Type	Received Signal	Tag 1	Tag 2	Tag 3	Tag 4	Tag 5	Tag 6	Tag 7	Tag 8
OCTAGONAL	Tag 1	**0.2092**	0.1946	0.1681	0.2053	0.1688	0.1795	0.171	0.1706
	Tag 2	0.1874	**0.2244**	0.1509	0.1832	0.1612	0.1693	0.1589	0.1853
	Tag 3	0.1466	0.1822	**0.2264**	0.1335	0.1618	0.1307	0.2047	0.2082
	Tag 4	0.1895	0.1724	0.1436	**0.2398**	0.1527	0.1612	0.1471	0.1546
	Tag 5	0.1535	0.166	0.1216	0.153	**0.2318**	0.1367	0.2181	0.1456
	Tag 6	0.1684	0.1408	0.1192	0.1766	0.1106	**0.1967**	0.1514	0.14
	Tag 7	0.1322	0.1832	0.1831	0.1319	0.1695	0.1266	**0.2912**	0.1719
	Tag 8	0.1446	0.1985	0.2088	0.134	0.1641	0.1225	0.1839	**0.2499**
CIRCULAR	Tag 1	0.3353	0.2961	0.2683	0.308	0.1871	0.2402	**0.3376**	0.3166
	Tag 2	**0.3266**	0.3219	0.227	0.2676	0.2263	0.2432	0.2708	0.2699
	Tag 3	0.2293	0.2434	0.2904	**0.383**	0.1579	0.1872	0.3276	0.3573
	Tag 4	0.2386	0.2189	0.2968	**0.4225**	0.19	0.2227	0.3546	0.3878
	Tag 5	0.28	**0.2892**	0.2269	0.2352	0.2284	0.1677	0.236	0.2484
	Tag 6	0.2941	0.289	0.1798	0.2491	0.1844	0.272	**0.2968**	0.2371
	Tag 7	0.3123	0.2621	0.2213	0.3224	0.1743	0.2633	**0.4411**	0.2969
	Tag 8	0.2464	0.2148	0.2805	**0.4177**	0.1928	0.2224	0.3368	0.3927

The detection results are resumed in Table 3-4, as can be seen the success of the detection decreases as the scenarios approaches the real case. The Octagonal Tags pass from a 100% detection rate in a noise and/or pathloss free scenario to only 25% for the real case, and for the Circular ones, the detection rate reduces from 62.5% to 25%.

Table 3-3. Correlation results for signals embedded in noise

Tag Type	Received Signal	Tag 1	Tag 2	Tag 3	Tag 4	Tag 5	Tag 6	Tag 7	Tag 8
OCTAGONAL	Tag 1	0.3026	0.2728	0.2662	0.3152	0.2553	0.3233	0.2665	**0.3397**
	Tag 2	0.303	0.2759	0.2599	0.3259	0.2736	0.3231	0.2768	**0.3402**
	Tag 3	0.2999	0.2914	0.2938	0.3221	0.263	0.3188	0.2843	**0.3546**
	Tag 4	0.3035	0.2723	0.2598	0.3108	0.2412	0.322	0.2745	**0.3509**
	Tag 5	0.2885	0.2598	0.2527	0.296	0.2635	0.3124	0.2758	**0.314**
	Tag 6	0.3101	0.2778	0.2433	0.3235	0.2363	0.317	0.2909	**0.359**
	Tag 7	0.3022	0.2899	0.2776	0.2995	0.2718	0.3171	0.3281	**0.3588**
	Tag 8	0.2976	0.3047	0.2877	0.3357	0.2718	0.3142	0.3051	**0.3633**
CIRCULAR	Tag 1	0.318	0.3133	0.2602	0.2592	0.1922	0.2407	**0.3597**	0.2591
	Tag 2	**0.3567**	0.3415	0.2463	0.2698	0.2315	0.2548	0.2954	0.2942
	Tag 3	0.2713	0.2898	0.3128	0.3301	0.1685	0.1856	**0.3364**	0.2976
	Tag 4	0.2274	0.2379	0.2911	**0.3654**	0.1994	0.2097	0.3523	0.3406
	Tag 5	**0.2969**	0.2802	0.2338	0.2518	0.236	0.203	0.2768	0.2677
	Tag 6	0.3254	0.2742	0.1982	0.2383	0.1939	0.2869	**0.3375**	0.2505
	Tag 7	0.301	0.2899	0.2371	0.2805	0.1807	0.2649	**0.4577**	0.2571
	Tag 8	0.2288	0.24	0.2655	**0.3575**	0.2015	0.2033	0.3292	0.3253

Table 3-4. Detected Tags for all three scenarios

Received Signal	Octagonal			Circular		
	Table 4.1	Table 4.2	Table 4.3	Table 4.1	Table 4.2	Table 4.3
Tag1	Tag1	Tag1	Tag8	Tag1	Tag7	Tag7
Tag2	Tag2	Tag2	Tag8	Tag2	Tag1	Tag1
Tag3	Tag3	Tag3	Tag8	Tag3	Tag4	Tag7
Tag4	Tag4	Tag4	Tag8	Tag4	Tag4	Tag4
Tag5	Tag5	Tag5	Tag8	Tag2	Tag2	Tag1
Tag6	Tag6	Tag6	Tag8	Tag7	Tag7	Tag7
Tag7	Tag7	Tag7	Tag8	Tag7	Tag7	Tag7
Tag8	Tag8	Tag8	Tag8	Tag4	Tag4	Tag4
Success (%)	100.0	100.0	25.0	62.5	25.0	25.0

3.2.2 Detection by means of Maximum Likelihood

The third detection algorithm is based on a statistical model, since in order to be able to implement it, the noise must be Gaussian distributed. The main idea is that the stored signal of any given tag (given by $\hat{\theta}$ in equation 3.4) that maximizes the likelihood function of the receive power, is the one as considered to be present in the detection zone.

$$\{\hat{\theta}_{mle}\}\{\text{argmax}_{\theta\in\,\Theta}\ \hat{l}\{\theta;\ s_1,\dots,s_n\}\} \quad (3.4)$$

Table 3-5. Maximum Likelihood results for noise and pathloss free signals

Tag Type	Received Signal	Tag 1	Tag 2	Tag 3	Tag 4	Tag 5	Tag 6	Tag 7	Tag 8
OCTAGONAL	Tag 1	**0**	0.0062	0.0071	0.0039	0.0123	0.0065	0.017	0.0152
	Tag 2	0.0062	**0**	0.0116	0.0114	0.0165	0.0117	0.0192	0.0096
	Tag 3	0.0071	0.0116	**0**	0.0123	0.0155	0.0146	0.01	0.0062
	Tag 4	0.0039	0.0114	0.0123	**0**	0.017	0.0072	0.0232	0.0197
	Tag 5	0.0123	0.0165	0.0155	0.017	**0**	0.0213	0.0108	0.0285
	Tag 6	0.0065	0.0117	0.0146	0.0072	0.0213	**0**	0.0244	0.0188
	Tag 7	0.017	0.0192	0.01	0.0232	0.0108	0.0244	**0**	0.0158
	Tag 8	0.0152	0.0096	0.0062	0.0198	0.0285	0.0188	0.0158	**0**
CIRCULAR	Tag 1	**0**	0.0039	0.0037	0.0061	0.0046	0.0038	0.0041	0.0049
	Tag 2	0.0039	**0**	0.004	0.0058	0.0016	0.0023	0.006	0.0054
	Tag 3	0.0037	0.004	**0**	0.0025	0.0039	0.0046	0.0041	0.0027
	Tag 4	0.0061	0.0058	0.0025	**0**	0.0059	0.0049	0.0041	0.0003
	Tag 5	0.0046	0.0016	0.0039	0.0059	**0**	0.0024	0.0062	0.0053
	Tag 6	0.0038	0.0023	0.0046	0.0049	0.0024	**0**	0.0031	0.0047
	Tag 7	0.0041	0.006	0.0041	0.0041	0.0062	0.0031	**0**	0.0045
	Tag 8	0.0049	0.0054	0.0027	0.0003	0.0053	0.0047	0.0045	**0**

Table 3-6. Maximum Likelihood results for Noise free signals

Tag Type	Received Signal	Tag 1	Tag 2	Tag 3	Tag 4	Tag 5	Tag 6	Tag 7	Tag 8
OCTAGONAL	Tag 1	0.0131	0.018	0.0158	0.0135	0.0217	**0.0114**	0.0269	0.0211
	Tag 2	0.0141	0.0162	0.0165	0.0146	0.0223	**0.0118**	0.0271	0.0193
	Tag 3	0.0147	0.0192	0.0138	0.0156	0.0226	**0.013**	0.0251	0.0186
	Tag 4	0.0143	0.0194	0.0172	0.0125	0.023	**0.0121**	0.0285	0.0223
	Tag 5	0.015	0.0195	0.0173	0.0155	0.0182	**0.0135**	0.0253	0.0237
	Tag 6	0.0148	0.0194	0.0176	0.0146	0.0238	**0.0108**	0.0287	0.0221
	Tag 7	0.0154	0.0193	0.0142	0.0165	0.0207	**0.0136**	0.0215	0.0185
	Tag 8	0.0161	0.0183	0.0146	0.0169	0.0247	**0.0136**	0.0255	0.0166
CIRCULAR	Tag 1	**0.0041**	0.0075	0.0086	0.0091	0.0115	0.0097	0.0075	0.0082
	Tag 2	0.0081	**0.0041**	0.0091	0.0092	0.009	0.0083	0.0095	0.0091
	Tag 3	0.0068	0.0074	**0.0043**	0.0049	0.0107	0.0101	0.0068	0.0053
	Tag 4	0.0091	0.0092	0.0065	**0.0036**	0.0125	0.0106	0.0072	0.0041
	Tag 5	0.0059	**0.0026**	0.0062	0.0065	0.0043	0.0056	0.0071	0.0062
	Tag 6	0.006	0.0043	0.0077	0.0065	0.0078	**0.0043**	0.0047	0.0066
	Tag 7	0.0078	0.0099	0.0087	0.0074	0.0132	0.0094	**0.0039**	0.008
	Tag 8	0.0079	0.0087	0.0064	**0.0036**	0.0118	0.0103	0.0074	0.0037

In short terms, a maximization of the likelihood function implies as the matter of fact that the final result should reach its minimum value. Therefore, as for the correlator detector

case, the studies were conducted using the three scenarios described in Figure 3-2. In Table 3-5 can be seen that for the case where the signal has been pre-processed by removing the noise and pathloss contributions, all signals are detected successfully and reaching a minimum value of zero in all cases and for both type of tags.

Table 3-6 shows the results for the noise free scenario, in the case of the Octagonal tags, only code 8 is successfully detected and for the circular ones, 7 codes are detected but code 5 which is confused by code 2.

Table 3-7 shows the results for the noisy scenario, in this case only code 4 is successfully detected for the Octagonal tags and 5 codes are successfully detected for the circular tags case.

Table 3-7. Maximum Likelihood results for signals embedded in noise

Tag Type	Received Signal	Tag 1	Tag 2	Tag 3	Tag 4	Tag 5	Tag 6	Tag 7	Tag 8
OCTAGONAL	Tag 1	0.0146	0.019	0.0188	**0.0079**	0.0262	0.0096	0.0324	0.0216
	Tag 2	0.0146	0.019	0.0188	**0.0079**	0.0262	0.0096	0.0324	0.0216
	Tag 3	0.0146	0.0191	0.0173	**0.0084**	0.0261	0.0098	0.0315	0.0201
	Tag 4	0.0148	0.0192	0.0183	**0.0079**	0.0264	0.0097	0.0316	0.0209
	Tag 5	0.0147	0.0196	0.0188	**0.008**	0.0242	0.0104	0.0316	0.0227
	Tag 6	0.014	0.0178	0.0178	**0.0077**	0.0248	0.0089	0.0305	0.0202
	Tag 7	0.0134	0.0178	0.0157	**0.0078**	0.0231	0.0091	0.028	0.0188
	Tag 8	0.0148	0.0185	0.017	**0.0089**	0.026	0.0101	0.0306	0.0189
CIRCULAR	Tag 1	**0.0061**	0.0096	0.0101	0.0114	0.0138	0.0112	0.0076	0.011
	Tag 2	0.0096	**0.0064**	0.0107	0.0117	0.0116	0.01	0.0096	0.0119
	Tag 3	0.0086	0.0095	**0.0061**	0.0075	0.0129	0.0116	0.0073	0.0083
	Tag 4	0.0101	0.0104	0.0075	**0.0059**	0.0143	0.0118	0.0074	0.0067
	Tag 5	0.0077	**0.0054**	0.008	0.0087	0.0074	0.0069	0.0066	0.009
	Tag 6	0.0088	0.0079	0.0105	0.0101	0.0119	0.0071	**0.0059**	0.0106
	Tag 7	0.0112	0.0133	0.0117	0.0112	0.0172	0.0126	**0.0059**	0.0122
	Tag 8	0.0086	0.0094	0.007	**0.0056**	0.0131	0.0111	0.0073	0.0059

The detection results are resumed in Table 3-8, as can be seen the success of the detection decreases as the scenarios approaches the real case. The Octagonal Tags pass from a 100% detection rate in a noise free scenario to only 12.5% for the pathloss free and real case scenarios. For the Circular ones, the detection rate reduces from 100% to 62.5%.

From the previous results, it could be inducted that an implementation of the correlation algorithm in a noise free scenario for the Octagonal tags and the Maximum likelihood in the noise embedded case for the Circular tags should be done. However, It is important to clarify that these results are based on the static case, that is, the tags are placed at a fixed position and measurements were taken. Furthermore, the presence of one of the tags in the detection zone is already known and the algorithms only need to detect which one it is, the case where no tag is present was evaluated during the final implementation of the algorithms in the respective readers.

Table 3-8. Maximum Likelihood detection success rate

Received Signal	Octagonal			Circular		
	Table 4.1	Table 4.2	Table 4.3	Table 4.1	Table 4.2	Table 4.3
Tag1	Tag1	Tag6	Tag4	Tag1	Tag1	Tag1
Tag2	Tag2	Tag6	Tag4	Tag2	Tag2	Tag2
Tag3	Tag3	Tag6	Tag4	Tag3	Tag3	Tag3
Tag4	Tag4	Tag6	Tag4	Tag4	Tag4	Tag4
Tag5	Tag5	Tag6	Tag4	Tag5	Tag2	Tag2
Tag6	Tag6	Tag6	Tag4	Tag6	Tag6	Tag7
Tag7	Tag7	Tag6	Tag4	Tag7	Tag7	Tag7
Tag8	Tag8	Tag6	Tag4	Tag8	Tag4	Tag4
Success (%)	100.0	12.5	12.5	100.0	75.0	62.5

3.3 Reader test beds

For both readers a simple common control console has been developed using the graphical user interface[5] from MATLAB, the display is shown in Figure 3-5. The interface plots the histogram that keeps track of the amount of detections performed to each code and also displays a symbolic picture that represents the detected code. The measurements start by pressing the "Run" button and can be stopped at any time by pressing the "Stop" Button.

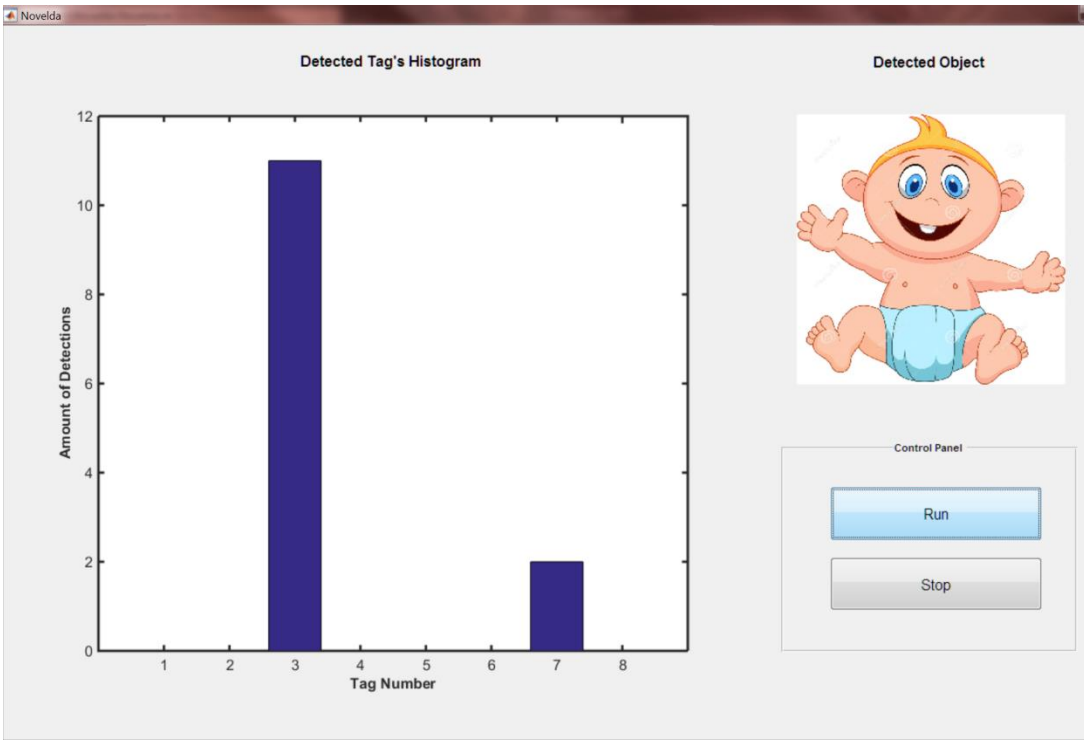

Figure 3-5. Display and control console of both the FD and TD Readers

Whenever no tag is present at the detection zone, the picture shown in Figure 3-6 is displayed.

[5] this Interface has been developed for testing purposes, but is not part of the COP or the eVACUATE final solution

Figure 3-6. No tag display picture

Figure 3-7: shows the different display pictures assigned to each of the codes present in the detection zone once they are detected: adult, child, baby, pregnant woman, handicap, crew member, official member, and rescue team member. These pictures can vary as required since they are only chosen for demonstration purposes.

(a)

(b)

(c)

(d)

(e)

(f)

(g)

(h)

Figure 3-7. Console display pictures for (a) code one, (b) code two, (c) code three, (d) code four, (e) code five, (f) code six, (g) code seven, and (h) code eight

The respective reader related developments are explained in the following subsections, specifically the ones concerning its calibration procedure and demonstration.

3.3.1 Frequency Domain Reader

The FD Reader is used for the detection of the circular tags, since its working principle is the same as for the lab equipment; the tags RF signature is loaded previously with the results obtained during the lab measurements. The Maximum Likelihood algorithm was implemented; a link to a video showing the working principle of the FD Reader can be found here under the name "FD_Reader" (annex A), the video (speed up 4 times) shows the capability of the Reader to detect individually at least **5 circular tags** under a real scenario. As can be seen, the tag can be perfectly held by hand during the experiment. A maximum reading distance of **30 cm** can be achieved.

3.3.2 Time Domain Reader (Novelda Radar)

This reader is used for the detection of the Octagonal tags; the calibration console is shown in Figure 3-8. The empty and reference measurements are taken by pushing the respective button under the required circumstances. Afterwards, each tag's signature is uploaded individually by selecting the corresponding tag in the list and pressing the "Load" button. In the same way, to view a specific tag characteristic the desired tag is selected from the list and the "View" button is pressed.

Both types of algorithms (correlation and maximum likelihood) were implemented and tested; the correlation algorithm couldn't produce any results because when evaluating the "no tag" case, this state prevailed over the others being unable to distinguish whether a tag was present or not in the detection zone. So finally de Maximum Likelihood for noise-free scenario was implemented. A link to a video showing the working principle of the TD Reader can be found here under the name "TD_Reader" (annex A), the video shows the capability of the Reader to detect individually up to **4 octagonal tags**. As can be seen, the tag can be perfectly held by hand during the experiment. A maximum reading distance of **50 cm** can be achieved.

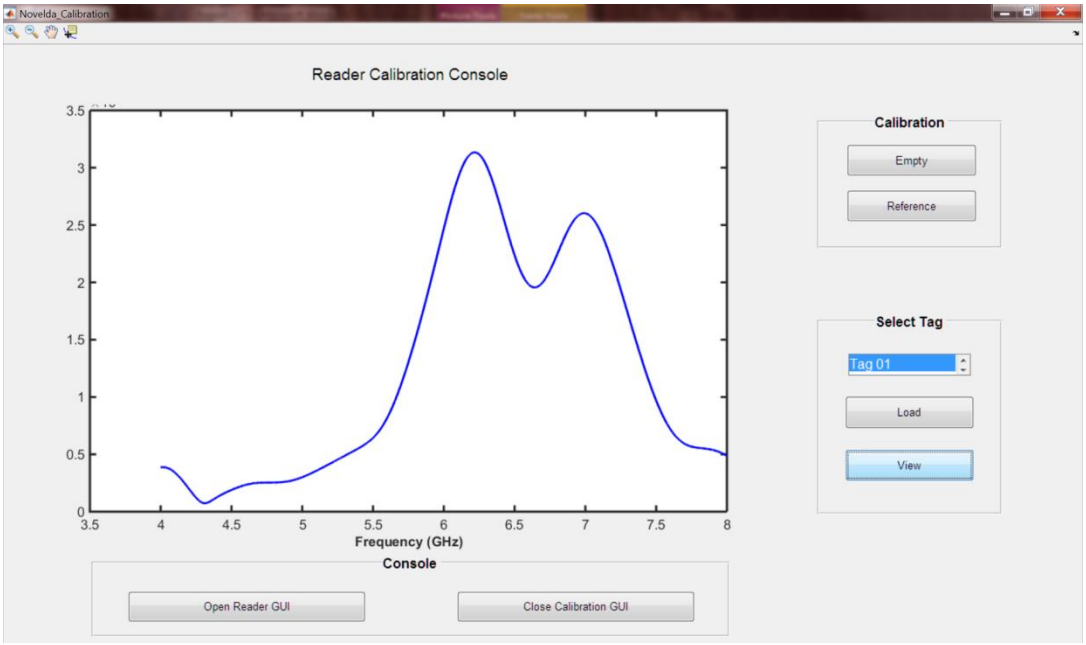

Figure 3-8. Display of the Graphical User Interface to calibrate the TD Reader

3.4 Anoeta Drill – Chipless RFID System report

On the sixth of December, 2015 the time domain Chipless RFID System based on the Novelda radar was tested at the Anoeta stadium venue located in San Sebastian, Spain. To perform the test, the RFID reader for chipless tags was placed at one of the gates as shown in Fig. 3-9.

Figure 3-9. Chipless RFID Reader placed at one of the gates of the Anoeta Stadium

This way the person coming out of the stadium can place the tag in the detection zone defined by the antennas, and its detected code can be shown in the laptop screen placed next to them.

Several tests were performed; either with the technical team of TU Dresden or with a volunteer's team of five persons, a video of the test performed by TUD can be found here. The results are in accordance with the technical assessments and tests done previously at the TU Dresden premises. Two rounds of tests T1 & T2 were performed with the volunteers showing a success rate between 0 – 80 % for each, the results are shown in Table 3-9.

Table 3-9. Test results with volunteers, T1: test 2 and T2: test 2

Code held	Code detected			
	Adult	Child	Baby	Pregnant
Adult	T1		T2	
Child	T2	T1		
Baby			T1,T2	
Pregnant		T1		T2
Child		T1,T2		

The observed reasons for the wrongful detection are the following reasons:

- The tag is removed too fast from the detection area.
- If the tag is not placed correctly in the detection area.
- Abrupt movement of the tag while is being detected.
- The tag detection is influenced by the body.

Therefore the use of the system needs to be taught to the end users and this should be taken into consideration for future tests.

The system worked as expected and further improvements needs to be done regarding the coding technique to improve the detection success rate, as well as to clearly delimitate the detection area to avoid placing the tag wrongfully since the antennas radiation pattern changes with the position and distance of the tag.

4 Conclusions

- The chipless RFID system has been developed according to the specifications defined in the DoW for the eVACUATE project. The system is composed by the chipless RFID tag and the associated reader.
- Two different chipless RFID tags were developed to fulfill the project requirements. The designed tags are the following: Octagonal chipless RFID tag and Circular chipless RFID tag (version 2). These chipless tags are fully printable and can be integrated in end-user items, such as tickets, associated cards etc. Roll-printing capability of chipless RFIDs has been proofed by screen printing as well as flexography.
- A test-bed for the chipless RFID reader has been developed. Two different approaches were followed to build the reader: A FMCW based radar (frequency-based) and an impulse based radar (time-based, also known as novelda-radar).
- A proof-of-concept in order to test the chipless RFID system was conceived. The proof-of concept system includes two variants: The frequency domain reader test-bed plus the circular chipless RFID tag, and the novelda-based test-bed plus the octagonal chipless RFID tags.
- The chipless RFID system is able to identify up to 8 different groups of people as required on the application, i.e. the developed tags have a minimum capacity of 3 bits as requested. High capacity tags, more commercial appealing, were also studied within the project.
- The price of the tags were evaluated and it was concluded that the objective price is not reachable with the current technology (2.15 €-Cent/tag for circular tags). Further alternatives, in order to reduce the fabrication cost were also studied with very promising results
- The life time of 3 months is guaranteed through the use of conductive inks with good environmental stability. Moreover, the application of protective coating to enlarge (even more) the life-time of the chipless RFID tags was studied.
- A read range up to 1.8 m for a chipless RFID tag has been demonstrated in anechoic chamber and an expected maximum read range, based on experimental results, of about 3.5 m can be estimated.
- A set of complementary performance test over the chipless RFID tag were performed. The additional test include: Bending and folding RF effects, Human body RF interference analysis, folding endurance and adhesion and abrasion tests.
- The initial results obtained during the Human body RF interference analysis suggest that that the use of the chipless RFID system in an emergency system may be limited in scope. Special situations as for instance, people carrying the tag in his pockets or near its body must be avoided. Further research to overcome this situation must be performed.
- A proof-of-concept chipless RFID system was successfully tested during the Anoeta Stadium's evacuation drill celebrated on the 6th December 2015.

5 References

[Ali14] M. Ali, D. Prakash, T. Zillger, P. K. Singh, and A. C. Hübler, “Printed Piezoelectric Energy Harvesting Device,” Adv. Energy Mater., vol. 4, no. 2, p. n/a–n/a, Jan. 2014.

[Bet15] D. Betancourt, R. Nair, K. Haase, G. Schmidt, M. Bellmann, D. Höft, A. Hübler, and F. Ellinger, “Square-shape fully printed chipless RFID tag and its applications in evacuation procedures,” in Proc. EUCAP2015, Lisbon, Portugal, 2015.

[Bos06] J. A. Bossard, D. H. Werner, T. S. Mayer, J. A. Smith, Y. U. Tang, R. P. Drupp, and L. Li, “The Design and Fabrication of Planar Multiband Metallodielectric Frequency Selective Surfaces for Infrared Applications,” IEEE Transactions on antennas and propagation, Vol. 54, No. 4, April 2006, pp. 1265-1276

[Bot_] Böttcher Siebdruck-Service GmbH, “SEFAR ® Gewebe + Technologie PET1500,” Datenblatt/Produktbeschreibung.

[Dup_] DuPont, “DuPont 5028 SILVER CONDUCTOR,” Tech. Data Sheet.

[ELA_] ELANTAS Beck GmbH, “Gravure or Flexo Printable Conductive Inks Bectron ® CP Series,” Tech. Inf.

[Fei07] M. K. Fein, A. Koptyug, and H. Nilsson, “Printed antennas with variable conductive ink layer thickness,” IET Microw. Antennas Propag., vol. 1, pp. 401–407, 2007.

[Hua15] X. Huang, T. Leng, X. Zhang, J. C. Chen, K. H. Chang, A. K. Geim, K. S. Novoselov, and Z. Hu, “Binder-free highly conductive graphene laminate for low cost printed radio frequency applications,” Appl. Phys. Lett., vol. 106, no. 20, p. 203105, May 2015.

[Karm13] N. Karmakar, R. Koswatta, P. Kalansuriya, and R. E-Azmin, Chipless RFID Reader Architecture, Artech House Publishers, 2013, ISBN: 168075613

[Kur15] KURZ, “Structure of hot stamping foil and self-adhesive label.” [Online]. Available: http://www.kurz.de/kurzweb/en/home.nsf/?Open&DirectURL=92603BF38CC03135C12570880033A2A4. [Accessed: 28-May-2015].

[Lya14] A. Lyashenko, “Untersuchung des Prägefoliendrucks im Hinblick auf die Anwendung im Elektronikbereich,” TU Darmstadt, 2014.

[Man09] M. Mäntysalo and P. Mansikkamäki, “An inkjet-deposited antenna for 2.4 GHz applications,” AEU - Int. J. Electron. Commun., vol. 63, no. 1, pp. 31–35, Jan. 2009.

[Nair14] R. Nair et al, “A Fully Printed Passive Chipless RFID Tag for Low-Cost Mass Production,” Proceedings of EUCAP2014, The Hague, Netherlands, pp. 2950-2954, April 2014.

[Nair14a] R. Nair et al, “A Novel Fully Printed 28-bits Capacity Chipless RFID Tag Based on Open Conical Resonators,” Proceedings of PIERS2014, Guangzhou, China, August 2014.

[PAR_] PARLEX Corporation, “Polymer Thick Film - Material Performance and Reliability,” Proced. Descr.

[Sid05] J. Siden, T. Olsson, A. Koptioug, and H. Nilsson, “Reduced Amount of Conductive Ink with Gridded Printed Antennas,” in Polytronic 2005 - 5th International Conference on Polymers and Adhesives in Microelectronics and Photonics, 2005, no. c, pp. 4–7.

[Tay12] D. Taylor, “Signal waveform variations in ultrawideband wireless systems: causes and aftereffects,” in Ultrawideband Radar: Applications and Design, CRC Press, 2012, pp. 71-104.

[Ven12] A. Vena, E. Perret, and S. Tedjini, “High Capacity Chipless RFID Tag Insensitive to the Polarization,” IEEE Transactions on Antennas and Propagation, Vol.60, No. 10, 2012, pp. 4509-4515.

Annex A – Link to support documents

List of videos		
1	Name	FD_Reader
	Type	wmv
	Link	https://exodusgr.sharepoint.com/eVACUATE/Shared%20Documents/Forms/AllItems.aspx?RootFolder=%2FeVACUATE%2FShared%20Documents%2FProject%20Officer%27s%20Folder%2FRFID%20Tags%20Multimedia&FolderCTID=0x01200028E3FD1578DCDE428A294756DEA23328&View=%7B2F821A6E-431A-4544-AC0F-6327207848FC%7D
2	Name	TD_Reader
	Type	wmv
	Link	https://exodusgr.sharepoint.com/eVACUATE/Shared%20Documents/Forms/AllItems.aspx?RootFolder=%2FeVACUATE%2FShared%20Documents%2FProject%20Officer%27s%20Folder%2FRFID%20Tags%20Multimedia&FolderCTID=0x01200028E3FD1578DCDE428A294756DEA23328&View=%7B2F821A6E-431A-4544-AC0F-6327207848FC%7D
3	Name	AnoetaTestTUD
	Type	wmv
	Link	https://exodusgr.sharepoint.com/eVACUATE/Shared%20Documents/Forms/AllItems.aspx?RootFolder=%2FeVACUATE%2FShared%20Documents%2FMultimedia%2FTUD-TUC&FolderCTID=0x01200028E3FD1578DCDE428A294756DEA23328&View=%7B2F821A6E-431A-4544-AC0F-6327207848FC%7D&InitialTabId=Ribbon%2ERead&VisibilityContext=WSSTabPersistence

Annex B – List of Acronyms

Acronym	Meaning
RFID	Radio Frequency Identification
AER	Active Evacuation Route
UWB	Ultra Wide Band
ETSI	European Telecommunications Standards Institute
Tx	Transmission
Rx	Reception
TUD	Technische Universität Dresden
TUC	Technische Universität Chemnitz
ID	Identification code
DoW	Description of Work Document
FSS	Frequency Selective Surface
CAD	Computer assisted design
PET	Polyethylene terephthalate
D7.3	Deliverable 7.3
D7.1	Deliverable 7.1
RF	Radio Frequency
IC	Integrated Circuit
FMCW	Frequency Modulated Continuous Wave
PC	Personal Computer
FPGA	Field Programmable Gate Array

Annex C – List of Units and Symbols

Acronym	Meaning
cm^2	Square centimetre
Und	unit
k	$1x10^3$
m	meter
V	Volts
GHz	Giga Hertz, $1x10^9$ Hertz
dBsm	Decibels per square meter
RCS	Radar Cross Section
µW	Micro Watt
dBi	Decibel over Isotropic antenna
VAC	Alternate Voltage
Kg	Kilogram
µm	Micro-meter
mm	Millimetre
Δ	delta
|RCS|	Magnitude of RCS
θ	Tilt angle
Ø	Diameter
MHz	Mega Hertz, $1x10^6$ Hertz
d	Conductor thickness
Ra, Rz,din	Roughness
$R_{\blacksquare}$	Sheet resistance
σ	Electrical conductivity
Δx, Δy	Printing accuracy